Cell

Identification of ALK in Thinness

Graphical Abstract

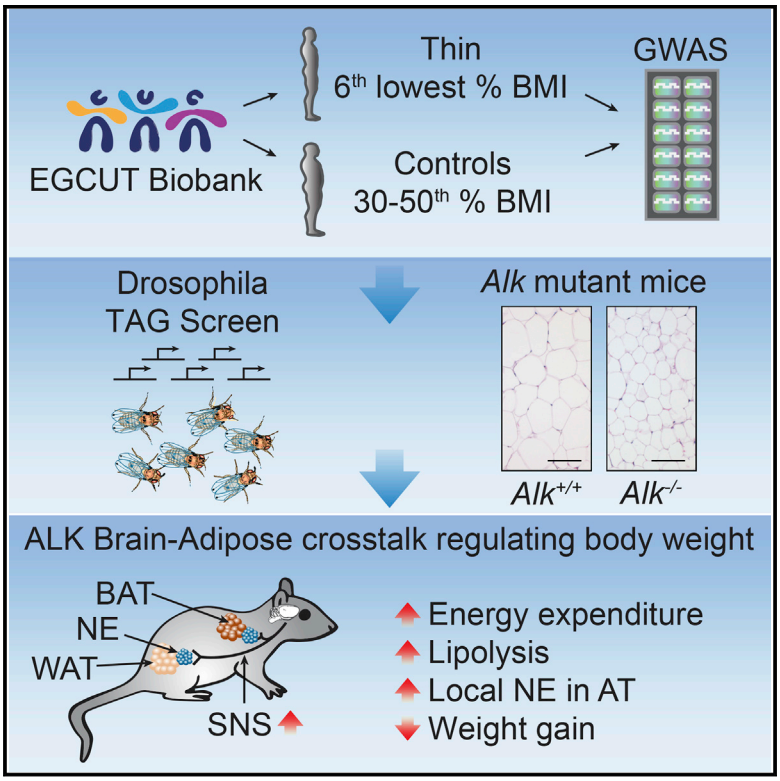

Highlights

- GWAS in the EGCUT biobank identifies *ALK* as a candidate thinness gene
- Knockdown of *Alk* in *Drosophila* results in reduced triglyceride levels
- *Alk* mutant mice exhibit resistance to diet- and leptin-mutation-induced obesity
- ALK controls energy expenditure via sympathetic tone to the adipose organ

Authors

Michael Orthofer, Armand Valsesia, Reedik Mägi, ..., Jorg Hager, Nele Gheldof, Josef M. Penninger

Correspondence

jorg.hager@rd.nestle.com (J.H.), josef.penninger@ubc.ca (J.M.P.), nele.gheldof@rd.nestle.com (N.G.)

In Brief

Genetic association studies in an Estonian biobank implicate ALK in the regulation of thinness. Studies in *Drosophila* and mice show that ALK functions as a regulator of sympathetic tone and loss of ALK leads to resistance to weight gain.

Orthofer et al., 2020, Cell *181*, 1246–1262
June 11, 2020
https://doi.org/10.1016/j.cell.2020.04.034

CellPress

Cell

Article

Identification of ALK in Thinness

Michael Orthofer,[1,21] Armand Valsesia,[2,21] Reedik Mägi,[3] Qiao-Ping Wang,[4] Joanna Kaczanowska,[5] Ivona Kozieradzki,[1] Alexandra Leopoldi,[1] Domagoj Cikes,[1] Lydia M. Zopf,[20] Evgenii O. Tretiakov,[6] Egon Demetz,[7] Richard Hilbe,[7] Anna Boehm,[7] Melita Ticevic,[1] Margit Nõukas,[3] Alexander Jais,[8] Katrin Spirk,[9] Teleri Clark,[10] Sabine Amann,[8] Maarja Lepamets,[3] Christoph Neumayr,[5] Cosmas Arnold,[5] Zhengchao Dou,[11,12] Volker Kuhn,[7] Maria Novatchkova,[5] Shane J.F. Cronin,[1] Uwe J.F. Tietge,[13,14] Simone Müller,[15] J. Andrew Pospisilik,[16] Vanja Nagy,[17] Chi-Chung Hui,[11,12] Jelena Lazovic,[20] Harald Esterbauer,[8] Astrid Hagelkruys,[1] Ivan Tancevski,[7] Florian W. Kiefer,[9] Tibor Harkany,[6,18] Wulf Haubensak,[5] G. Gregory Neely,[10] Andres Metspalu,[3] Jorg Hager,[2,*] Nele Gheldof,[2,*] and Josef M. Penninger[1,19,22,*]

[1]IMBA, Institute of Molecular Biotechnology of the Austrian Academy of Sciences, Vienna 1030, Austria
[2]Metabolic Phenotyping, Nestlé Research, EPFL Innovation Park, Lausanne 1015, Switzerland
[3]Estonian Genome Center, Institute of Genomics, University of Tartu, Tartu 51010, Estonia
[4]School of Pharmaceutical Sciences (Shenzhen), Sun Yat-sen University, Guangzhou 510275, China
[5]IMP, Institute of Molecular Pathology, Vienna 1030, Austria
[6]Department of Molecular Neurosciences, Center for Brain Research, Medical University of Vienna, Spitalgasse 4, Vienna 1090, Austria
[7]Department of Internal Medicine II, Innsbruck Medical University, Innsbruck 6020, Austria
[8]Department of Laboratory Medicine, Medical University of Vienna, Vienna 1090, Austria
[9]Division of Endocrinology and Metabolism, Department of Medicine III, Medical University of Vienna, Vienna 1090, Austria
[10]Dr. John and Anne Chong Lab for Functional Genomics, Charles Perkins Centre, Centenary Institute, and School of Life and Environmental Sciences, University of Sydney, Camperdown, NSW 2006, Australia
[11]Program in Developmental & Stem Cell Biology, The Hospital for Sick Children, Toronto, ON M5G 0A4, Canada
[12]Department of Molecular Genetics, University of Toronto, Toronto, ON M5S 1A8, Canada
[13]Division of Clinical Chemistry, Department of Laboratory Medicine, Karolinska Institute, 141 52 Huddinge, Sweden
[14]Clinical Chemistry, Karolinska University Laboratory, Karolinska University Hospital, 141 86 Stockholm, Sweden
[15]Institute of Animal Breeding and Genetics, University of Veterinary Medicine Vienna, Veterinärplatz 1, 1210 Vienna, Austria
[16]Center for Epigenetics, Van Andel Research Institute, Grand Rapids, MI 49503, USA
[17]Ludwig Boltzmann Institute for Rare and Undiagnosed Diseases, 1090 Vienna, Austria
[18]Section for Chemical Neurotransmission, Department of Neuroscience, Biomedicum 7D, Solnavägen 9, 17165 Solna, Sweden
[19]Department of Medical Genetics, Life Science Institute, University of British Columbia, Vancouver, BC V6T 1Z3, Canada
[20]Vienna BioCenter Core Facilities GmbH (VBCF), Vienna 1030, Austria
[21]These authors contributed equally
[22]Lead Contact
*Correspondence: jorg.hager@rd.nestle.com (J.H.), nele.gheldof@rd.nestle.com (N.G.), josef.penninger@ubc.ca (J.M.P.)
https://doi.org/10.1016/j.cell.2020.04.034

SUMMARY

There is considerable inter-individual variability in susceptibility to weight gain despite an equally obesogenic environment in large parts of the world. Whereas many studies have focused on identifying the genetic susceptibility to obesity, we performed a GWAS on metabolically healthy thin individuals (lowest 6th percentile of the population-wide BMI spectrum) in a uniquely phenotyped Estonian cohort. We discovered anaplastic lymphoma kinase (*ALK*) as a candidate thinness gene. In *Drosophila*, RNAi mediated knockdown of *Alk* led to decreased triglyceride levels. In mice, genetic deletion of *Alk* resulted in thin animals with marked resistance to diet- and leptin-mutation-induced obesity. Mechanistically, we found that ALK expression in hypothalamic neurons controls energy expenditure via sympathetic control of adipose tissue lipolysis. Our genetic and mechanistic experiments identify *ALK* as a thinness gene, which is involved in the resistance to weight gain.

INTRODUCTION

The prevalence of obesity and health-associated complications continue to rise throughout the world (Abarca-Gómez et al., 2017). Body mass index (BMI), commonly used to classify weight categories, is a highly complex trait that integrates the action of many genes and environmental cues (Maes et al., 1997). Recent developments of large genome-wide association studies (GWASs) have significantly enhanced our understanding of the genetic variants involved in polygenic obesity (Locke et al., 2015). Despite the fact that more than 700 common SNPs have been linked to BMI (Yengo et al., 2018a), only a limited number of genes involved in human body weight regulation have been identified and validated to date, including *MC4R* (Huszar et al., 1997; Lotta et al., 2019), *POMC* (Yaswen et al., 1999), and *SH2B1* (Ren et al., 2007). Though most studies in the field

have focused on the susceptibility to obesity, only few have explored the genetics of thinness, either in humans (Bulik and Allison, 2001; Laskarzewski et al., 1983; Lu et al., 2016; Magnusson and Rasmussen, 2002; Ran et al., 2017; Riveros-McKay et al., 2019; Zillikens et al., 2017) or in polygenic lean mouse models (Horvat et al., 2000; Morton et al., 2005). However, few of these studies provided any direct functional evidence linking human data to identification of potential gene(s) involved in the resistance to weight gain.

To further investigate the role of genetics in body weight regulation, we explored the human phenotype of persistent extreme low BMI (defined as BMI below the population-wide 6th percentile, adjusted for gender and age, generally corresponding to BMI lower than 18 kg/m^2) (Apfelbaum and Sachet, 1982; Estour et al., 2014). We performed a GWAS comparing thin with control individuals. We discovered that variants within the *ALK* gene are associated with the thinness phenotype. *ALK* is frequently mutated in various types of cancer (Della Corte et al., 2018), thereby having gained prominence as a key oncogenic driver; however, the physiological role of ALK outside of cancer has remained largely unclear. Using multiple independent genetic mouse models, we show that knock out of ALK results in thin animals resistant to diet-induced obesity with many striking similarities to the human thinness phenotype.

RESULTS

GWAS for Human Thinness

To identify variants associating with thinness, we performed a GWAS between groups belonging to different categories of the population-wide BMI spectrum in Estonia. The Estonian biobank (Estonian Genome Center of the University of Tartu; EGCUT) contains one of the largest and best phenotyped population cohort data in the world (www.biobank.ee), enabling us to use stringent and well-defined criteria that exclude samples from people with diseases such as lipodystrophy or anorexia nervosa (Figure 1A; see STAR Methods and Table S1 for detailed exclusion criteria). Population-wide BMI distributions are greatly affected by age and gender (Bulik and Allison, 2001). Therefore, rather than using strict BMI cutoffs, we selected individuals based on age- and gender-adjusted BMI. Control individuals were within the 30–50th percentile, thin individuals belonged to the lowest 6th percentile, and obese individuals to the highest 95th percentile of the population-wide BMI range grouped by age and gender (Figure S1). Based on these criteria, we classified ~1.9% of the cohort as "thin individuals."

Case-control GWAS analysis of the thin-versus-control individuals identified a distinct set of variants reaching $p < 10^{-5}$ (Figure 1A; Table S1). When comparing control versus obese individuals in the EGCUT dataset, we found among the top variants the well-known BMI-associated variants such as *FTO* and *MC4R* (Figure 1B; Table S1). Of the top five genomic loci associating with thinness versus controls (Table 1), two loci were located between genes (between *ICE1* and *MED10*, and *FOS* and *TMED10*). Furthermore, we found association of the thinness phenotype with a variant in an uncharacterized lncRNA (long non-coding RNA), AC013652.1. Two variants were located within genes: rs79938778 within *DEPTOR* and rs568057364 located in the first intron of *ALK*. Interestingly, the *ALK* rs568057364 variant is in strong linkage disequilibrium (LD) with another thinness-associated *ALK* variant rs202021741 (Figure 2A; Table S1). Genotype frequencies of these two *ALK* variants in the thin and control group are shown in Figure S2A. Principal component analysis of the two *ALK* variants identified in the Estonian population did not reveal abnormal stratification in different populations; both indels are common in European, Asian, as well as admixed American populations but less frequent in African ancestry populations (Figure S2B). *DEPTOR* is a negative regulator of the mTOR signaling pathway which, in mouse studies, was identified as a regulator of adipogenesis (Laplante et al., 2012) and in the protection against high-fat diet (HFD)-induced obesity when overexpressed in the hypothalamus (Caron et al., 2015). *ALK* has been extensively studied in cancer, but little is known about the biological role of *ALK* outside the context of cancer.

Prioritization of Candidate Genes Using *Drosophila* Genetics and GWAS Data Mining

Next, we used *Drosophila* genetics to prioritize potential genes for follow-up studies. We therefore determined whether the genes in the vicinity of the thinness variants regulate fat metabolism. Briefly, we identified 38 human genes that are within ~1Mb of the top five thinness-associated loci, determined their orthologs in flies, performed RNAi-mediated knockdown in *Drosophila*, and evaluated the effect on whole-body triglyceride levels (Figure 2B; Table S2). Of the 24 orthologous genes, knockdown of 5 genes resulted in significantly lower triglyceride accumulation: the fly orthologs of the transcription factors ZC2HC1C (CG42675) and MEIS2 (hth), the metallopeptidase ADAMTS16 (AdamTS-A), the DNA polymerase PAPD7 (Trf4-2) involved in DNA repair, and, importantly, ALK (Alk). In multiple repeat experiments, we confirmed that knockdown of Alk results in reduced triglyceride levels using normal- as well as high-sucrose diets (Figure 2C). Of note, *Alk* RNAi flies showed normal food intake but exhibited a mild reduction in lifespan compared to the parental control Actin-Gal4 line (Figures S2C and S2D), indicating metabolic dysregulation. Overexpression of *Alk* had no apparent effect on triglyceride levels and lifespan (Figures S2E and S2F). Thus, knockdown of fly orthologs of genes near the human GWAS variants from the Estonian thinness cohort affect triglyceride levels in *Drosophila*.

As a next prioritization step for these five candidate genes, we queried GWAS data as well as prior metabolic phenome-wide associations (Table S2). We found that only two of these five genes have been associated with defined metabolic traits. For *MEIS2*, one metabolic trait (waist circumference) has been reported. Importantly, our data mining showed that multiple metabolic traits have been associated with the *ALK* locus, including BMI, plasma triglyceride levels, plasma LDL cholesterol levels, glucose homeostasis, plasma adiponectin levels, and glycated hemoglobin (Figure 2A; Table S2). Of note, applying the same stringent selection criteria of our GWAS (6th percentile lowest BMI and exclusion criteria) to the UKBB data to categorize thin individuals, we found no significant association with thinness for the two *ALK* variants (imputation score > 90% for both indels) identified in the Estonian cohort. However, the association of

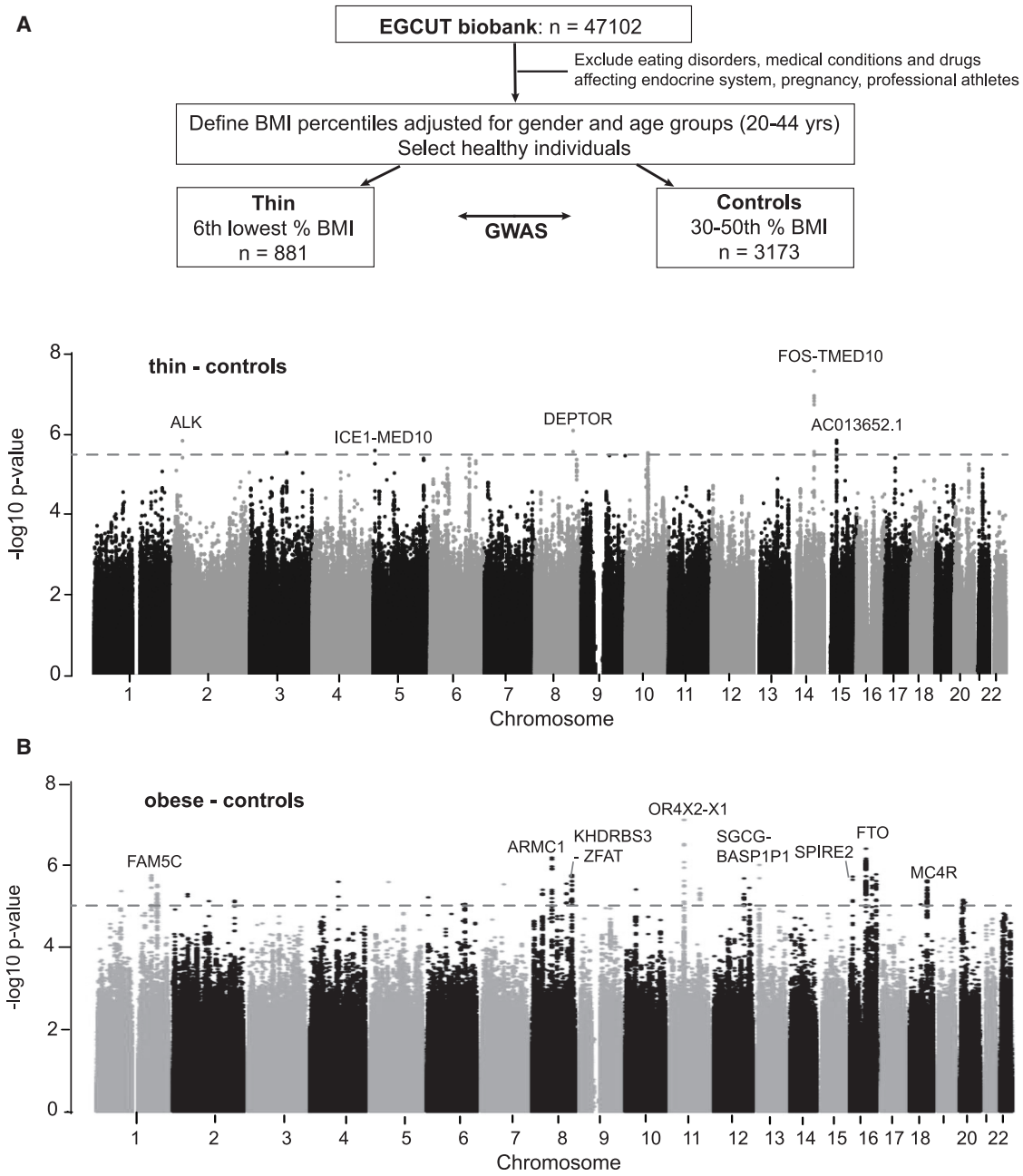

Figure 1. GWAS in the Estonian Population Shows Association of Variants with Thinness

(A) Outline of the selection of thin and control individuals from a population-wide cohort, with Manhattan plot (bottom panel) showing the significance of association between all variants and the thinness phenotype versus controls. Grey dotted line indicates discovery significance threshold at p = 1e-5.

(B) Manhattan plot showing the significance of association between all variants and the same control versus obese individuals selected from the EGCUT biobank. Grey dotted line indicates significance threshold at p = 1e-5. Names of the genes nearby the top variants are indicated.

See also Figure S1 and Table S1.

other variants within the *ALK* locus with BMI was found in two major, publicly available resources, namely the UKBB and the GIANT consortium (see above). Thus, our new EGCUT data and mining of the GWAS catalog showed that several variants within *ALK* are associated with different metabolic traits such as thinness, BMI, and lipid and glucose homeostasis.

Alk Knockout Mice Are Thin

Given that we found that the *ALK* locus is associated with multiple metabolic phenotypes in human and that knockdown of *Alk* results in reduced triglyceride accumulation in the fly, we focused our functional characterization on this gene. ALK is a member of the insulin receptor superfamily (Iwahara et al.,

Table 1. Processed GWAS Hits with Top Five Loci Showing Each Time the Top Thinness-Associated Variant within Each Locus

Variant ID	Chr	Position (bp)	Location	Nearest Gene	Effect Allele Frequency	Effect Allele	Non-effect Allele	Odd ratio (95% CI)	p Value
rs6574213	14	75697051	intergenic	*FOS, TMED10*	0.28	G	A	0.7 (0.61,0.79)	2.6E-08
rs79938778	8	121027633	intronic	*DEPTOR*	0.05	T	C	0.48 (0.35,0.66)	8.0E-07
rs61685635	15	39435617	intronic	*AC013652.1* (lncRNA)	0.07	A	T	0.56 (0.43,0.72)	1.4E-06
rs568057364	2	30025643	intronic	*ALK*	0.47	CT	C	1.33 (1.18,1.49)	1.4E-06
rs4521442	5	5853519	intergenic	*ICE1, MED10*	0.35	C	T	1.32 (1.18,1.48)	2.5E-06

Abbreviations: Chr, chromosome; CI, confidence interval; *FOS*, Fos proto-oncogene AP-1 transcription factor subunit; *TMED10*, transmembrane P24 trafficking protein 10; *DEPTOR*, DEP domain-containing MTOR interacting protein; AC013652.1, uncharacterized long non-coding RNA (lncRNA); *ALK*, anaplastic lymphoma kinase; *ICE1*, interactor of little elongation complex ELL subunit 1; *MED10*, mediator complex subunit 10.
See also Figure 1 and Table S1.

1997; Morris et al., 1994), first described as an oncogene resulting from a t(2;5)(p23;q35) *NPM1/ALK* chromosomal translocation in anaplastic large-cell non-Hodgkin's lymphomas (Morris et al., 1994). More than 20 different *ALK* rearrangements and mutations have been reported in tumors including neuroblastomas and non-small cell lung cancers (Della Corte et al., 2018; Hallberg and Palmer, 2016). Based on the expression of its mRNA throughout the nervous system during embryogenesis and also in the adult brain, mammalian ALK is thought to play a role in the development and function of the nervous system (Iwahara et al., 1997; Vernersson et al., 2006). However, besides subtle behavioral alterations observed in *Alk* deficient mice (Bilsland et al., 2008; Lasek et al., 2011a; Mangieri et al., 2017; Weiss et al., 2012), these mice are viable and fertile, showing no obvious phenotypes. Interestingly, one study noted a small difference in body weight of *Alk* deficient mice but did not further explore these preliminary findings (Bilsland et al., 2008). Therefore, we performed an in-depth analysis of *Alk* knockout ($Alk^{-/-}$) mice and also generated a new, independent mutant mouse line for tissue-specific *Alk* deletion to assess the role of ALK in metabolism.

Alk mutant mice were born at the expected Mendelian ratio (Figure S3A), and loss of *Alk* had no apparent effect on anxiety (open field test); locomotion, coordination, and balance (rotarod test); pain perception (hot plate and tail flick tests); fertility; physical appearance; tissue morphology; blood composition; or serum chemistry (Figures S3B–S3E; Table S3). Next, we recorded body weights of male and female $Alk^{+/+}$ and $Alk^{-/-}$ mice fed a standard chow diet (SD). Mice of both genotypes were born with similar weights but $Alk^{-/-}$ mice developed a thin phenotype at the age of 5 weeks, persisting into adulthood (Figure 3A; Figure S3F) while body length was normal (Figure S3G). Analysis of lean and fat mass by magnetic resonance imaging (MRI) and quantification of epididymal and subcutaneous white adipose tissue (epWAT and scWAT) revealed a reduced body adiposity in $Alk^{-/-}$ compared to $Alk^{+/+}$ mice while lean mass was similar (Figures 3B and 3C). Furthermore, adipocytes from $Alk^{-/-}$ epWAT and scWAT depots displayed a markedly reduced cell size (Figure 3D), indicating reduced lipid accumulation.

We examined the daily food intake of single housed $Alk^{+/+}$ and $Alk^{-/-}$ mice over several weeks but did not observe a difference between genotypes (Figure 3E). Intestinal lipid absorption and levels of neutral sterols and bile acid content in the feces were unchanged in $Alk^{-/-}$ mice as compared to littermate controls (Figures S3H and S3I), suggesting normal intestinal digestion and absorption of fat in *Alk*-deficient mice. Daily activity was also not changed in $Alk^{-/-}$ mice (Figure 3F). In line with reduced body weight, *Alk* mutant mice exhibited improved glucose tolerance (Figure 3G). Notably, adiponectin levels were increased in $Alk^{-/-}$ mice (Figure 3H). Importantly, male $Alk^{-/-}$ mice housed at thermoneutrality (30°C), the optimal housing temperature to mimic the thermal environment of humans (Fischer et al., 2018), showed reduced weight gain compared to $Alk^{+/+}$ mice (Figure 3I). These results, in line with our human GWAS and fly data, show that $Alk^{-/-}$ mice on standard chow diet exhibit a thin phenotype, elevated adiponectin levels, and improved glucose homeostasis, while having unaltered food intake and activity.

Genetic Deletion of *Alk* Increases Energy Expenditure and Confers Resistance to Obesity

Constitutionally thin individuals show a resistance to weight gain following a fat overfeeding period (Germain et al., 2014). To determine if $Alk^{-/-}$ mice resist weight gain, we mimicked caloric overload by challenging adult mice with a HFD for 16 weeks. Intriguingly, *Alk* knockout mice were significantly protected against HFD-induced obesity (Figures 4A and 4B). Of note, $Alk^{+/-}$ mice also showed reduced body weight gain on HFD compared to $Alk^{+/+}$ mice (not shown), indicative of a gene-dosage effect. To confirm these findings in an independent *Alk* mutant mouse line, we generated *Alk* conditional knockout mice (Figures S4A and S4B). Floxed mice crossed to transgenic animals expressing Cre recombinase under the ubiquitous actin promoter ($Alk^{fl/fl}$ *ActinCre*$^{+}$) recapitulated the resistance to HFD-induced obesity observed in conventional $Alk^{-/-}$ mice (Figure 4C). Moreover, similar to diet-induced obesity, *Alk* deficiency led to a significantly reduced weight gain in the genetic obesity model of leptin deficiency (*ob/ob*) (Figure 4D).

Next, we assessed body composition of mice by MRI. $Alk^{-/-}$ mice fed HFD displayed normal lean mass but a strong reduction in adiposity (Figures 4E–4G) and smaller adipocytes in both epWAT and scWAT compared to HFD-fed $Alk^{+/+}$ mice (Figure 4H; Figure S4C), while daily caloric intake of individually housed

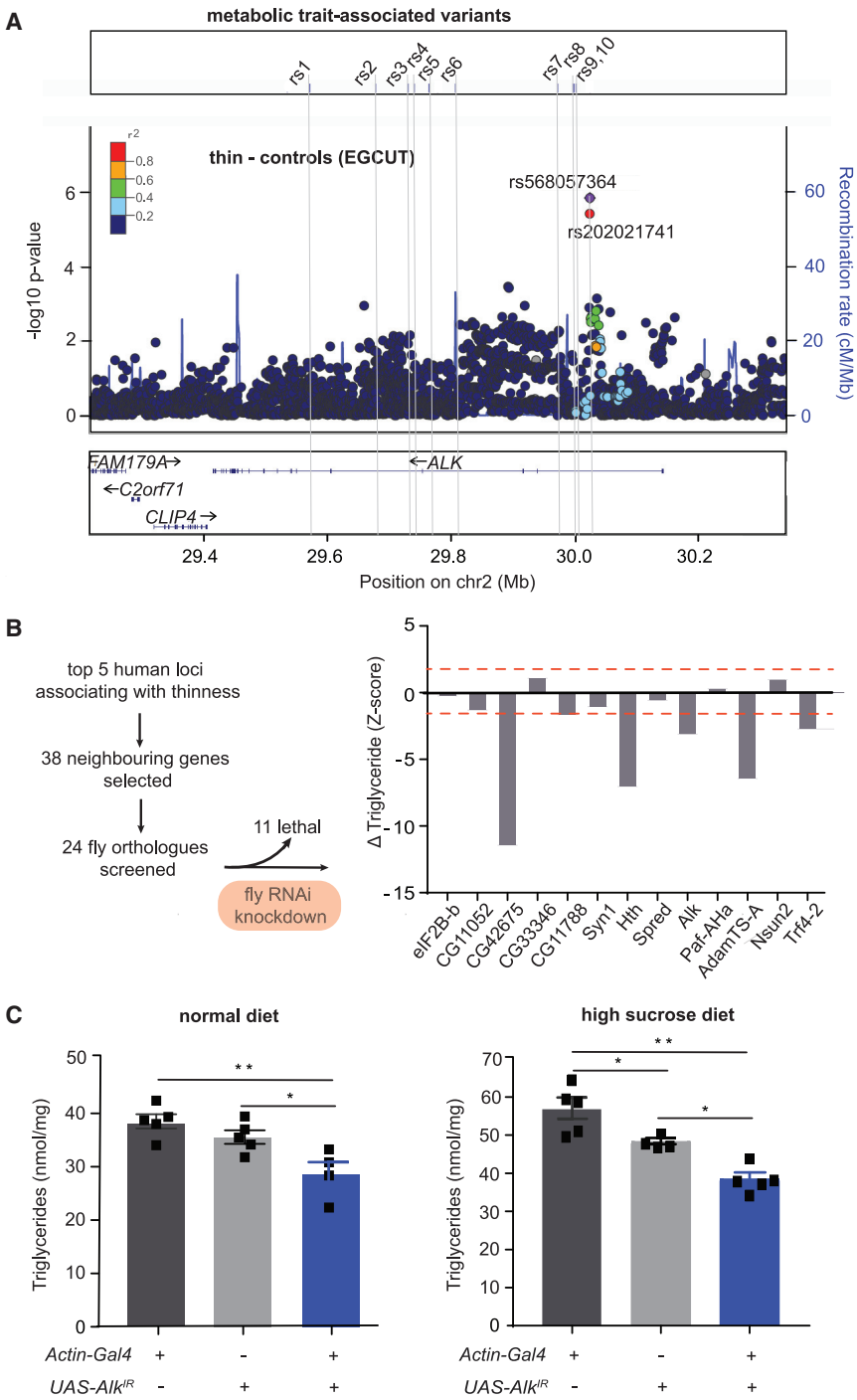

Figure 2. Targeted Fly RNAi Screen Shows that *Alk* Regulates Triglyceride Levels

(A) Locus zoom plot around the *ALK* locus showing the two variants within the first intron of *ALK* specific to the thin versus controls in the EGCUT data. The top panel shows the location of 10 variants within *ALK* that have previously been described to significantly associate with metabolic traits. Variant position is indicated on the x axis, statistical significance (−log10 p value) on the y axis. Each point corresponds to a variant. The top associated variant is indicated with a diamond shape (in purple). Variants are colored based on the index variant with which they are in strongest linkage disequilibrium. Gene positions are indicated in the lower panel. The peak lines in the upper panel (secondary y axis on the right) indicate recombination rates (in centimorgans per megabase).

(B) The nearby genes around the top five variants associating with thinness in human were evaluated for conservation level in fly (DIOPT score), and highly conserved genes were chosen for targeted RNAi knockdown in *Drosophila melanogaster*. Body weight and triglyceride levels of 4-day-old F1 adult male flies were measured and Z-score for each UAS-RNAi was calculated. Data are expressed as *Z* scores and *Z* score $\geq$ 1.96 or *Z* score $\leq$ −1.96 (red dotted lines indicate threshold) was considered a significant hit (n = 40 flies per group).

(C) Whole-body RNAi knockdown of *Alk* decreases triglyceride levels in both normal diet (left panel) and high sucrose diet (right panel) (n = 4–7 groups, 5 flies per group).

Data are represented as mean ± SEM.; *p < 0.05, **p < 0.01. One-way ANOVA with Bonferroni's multiple comparisons test (C).See also Figure S2 and Table S2.

mice was not different (Figure 4I). In accordance with unaltered food intake but reduced weight gain, *Alk*-deficient mice showed reduced feeding efficiency (Figure 4J), a measure of mg body weight gain per kcal food intake. To unravel the resistance to diet-induced weight gain in *Alk* knockout mice, we measured energy expenditure (EE) using indirect calorimetry. Plotting of individual data points revealed that $Alk^{-/-}$ mice have an elevated daily EE compared to $Alk^{+/+}$ mice (Figure 4K), suggesting excess catabolism as the potential cause of the adiposity resistant phenotype. We did not observe any apparent difference in daily circadian activity between the cohorts analyzed (Figure S4D). Glucose tolerance was markedly improved in $Alk^{-/-}$ mice versus $Alk^{+/+}$ mice fed the HFD (Figure S4E). Plasma adiponectin levels were also increased in HFD-fed mutant mice (Figure S4F). Various ligands for ALK have been reported, including pleiotrophin (*Ptn*) (Stoica et al., 2001), midkine (*Mdk*) (Stoica et al., 2002), heparin (Murray et al., 2015), and ALK and LTK ligand 1 and 2 (*Alkal1* and *Alkal2*) (Guan et al., 2015). We combined single and double mutants for *Mdk* and/or *Ptn* with *Alk* knockouts and found that loss of *Alk* still diminished HFD-induced obesity in the absence of both ligands (Figures S4G–S4I), suggesting that other ligands might be involved. Thus, *Alk*-deficient mice exhibit increased energy expenditure and are markedly protected against HFD- and genetically induced obesity.

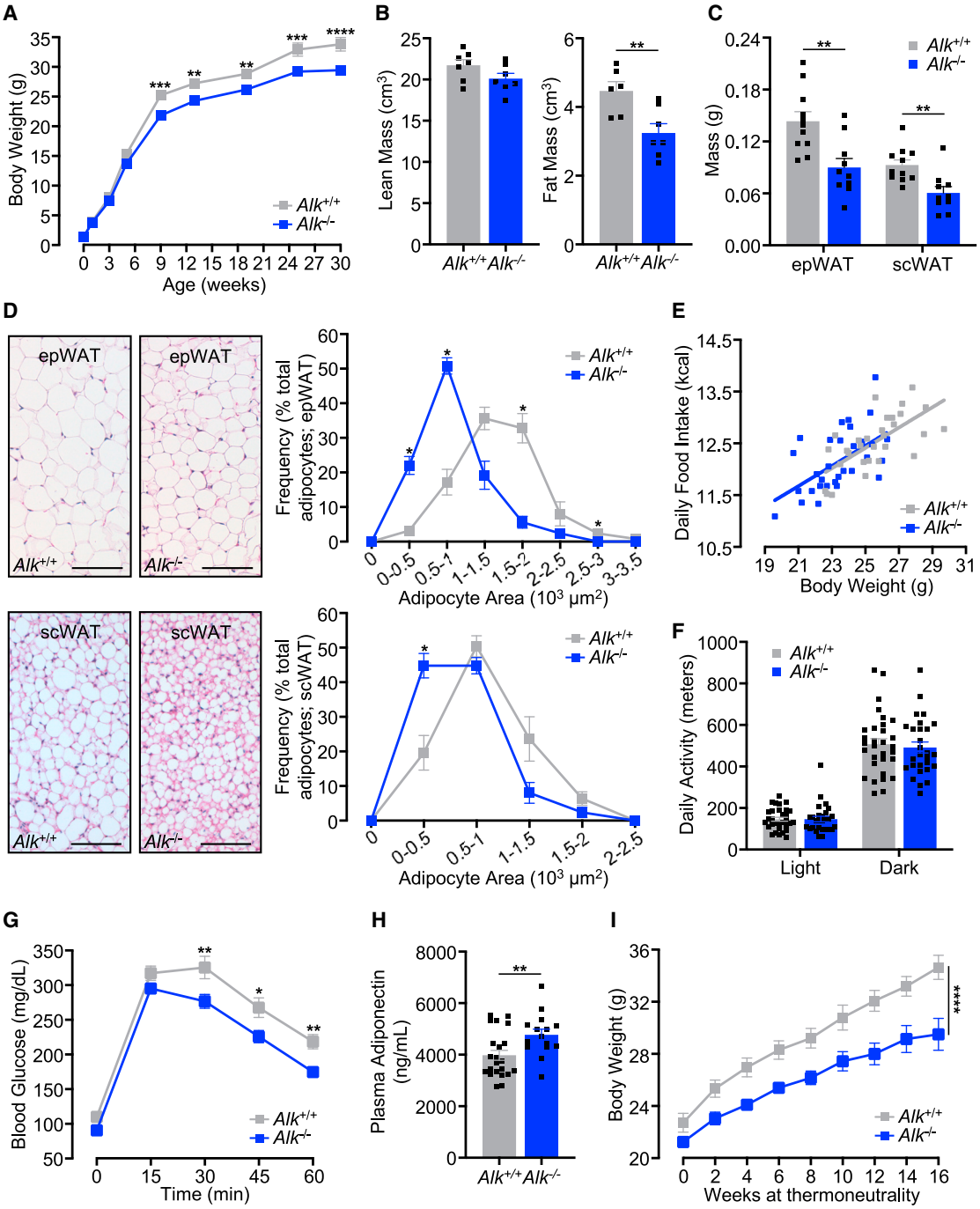

Figure 3. *Alk* Knockout Mice on Standard Chow Diet Are Thin

(A) Body weight curves of male $Alk^{+/+}$ and $Alk^{-/-}$ mice on standard chow diet (SD) (n ≥ 11).

(B) Lean and fat mass of mice measured by MRI (n = 7; 6 months old).

(C) Quantification of epWAT and scWAT depots (n ≥ 10; 16 weeks old).

(D) Representative pictures of hematoxylin and eosin stained adipose tissue sections (left panels) and analysis of adipocyte size (right panel) of epWAT and scWAT (n = 5; 18 weeks old). Scale bar: 100 µm.

(E) Daily food intake of single-caged $Alk^{+/+}$ and $Alk^{-/-}$ littermate mice plotted against body weight (n ≥ 17; 1 to 3 data points per mouse).

(F) Analysis of daily activity stratified by light and dark phases (n ≥ 28).

(G) Blood glucose levels of SD fed mice following an oral glucose bolus (n ≥ 21).

(legend continued on next page)

Alk Acts in the Central Nervous System

To gain further insight into ALK-mediated control of weight gain, we examined *Alk* mRNA expression in a mouse tissue library and observed high levels of *Alk* mRNA in cerebellum, cortex, and especially hypothalamus of the central nervous system (Figure S5A). Notably, we did not detect *Alk* expression in key metabolic tissues such as liver, muscle, WAT, and brown adipose tissue (BAT) (Figure S5A). To further analyze *Alk* expression, we took advantage of the lacZ cassette inserted into the *Alk* locus in our conventional knockout mice ($Alk^{-/-}$). X-gal staining of $Alk^{-/-}$ mice revealed strong lacZ expression in the paraventricular nucleus (PVN) of the hypothalamus (Figure 5A), a brain center where numerous afferent neuronal circuits converge to regulate energy balance via hormonal output pathways and sympathetic tone (Cowley et al., 1999; Foster et al., 2010; Hill, 2012; Williams et al., 2001). Comparable *Alk* expression in the PVN can also be seen in the Allen brain atlas (http://mouse.brain-map.org/). Quantification of hypothalamic mRNA levels in fasted and refed $Alk^{+/+}$ mice showed that *Alk* mRNA expression was induced in response to feeding (Figure 5B). In human, *ALK* is also highly expressed in the hypothalamus (http://gtexportal.org).

To further characterize Alk^{+} neurons in the PVN, we employed single-cell RNA-sequencing (10x Genomics on 11,380 cells of ectodermal origin) in postnatal mice (P10–23). We used published criteria on hypothalamic neuronal heterogeneity (Simmons and Swanson, 2009) to separate magnocellular neuroendocrine oxytocin (mneOXY), magnocellular neuroendocrine vasopressin (mneVAS), parvicellular neuroendocrine corticotropin-releasing hormone (pneCRH), parvicellular neuroendocrine somatostatin (pneSS), and parvicellular neuroendocrine thyrotropin-releasing hormone (pneTRH) neurons (Figure 5C; Figures S5B and S5C). Out of the 514 neurons we were able to assign to PVN origin, 223 also expressed *Alk*. Further fine mapping showed that most Alk^{+} cells are excitatory glutamatergic neurons based on their co-expression of *Slc17a6* (*Vglut2*; Figure 5D, left panel). Alk^{+} neurons were largely negative for *Gad1* (Figure 5D, middle panel), a marker for inhibitory GABA neurons. Among the five subtypes of PVN neurons, Alk^{+} neurons preferentially correspond to pneSS neurons (Figure 5D, right panel) and to a lesser extent to pneCRH neurons (Figure S6A). Among pneTRH, mneOXY, and mneVAS neurons, *Alk* can be expressed, but neither positive nor strong correlation was observed (Figures S6B–S6D). Using *UpSet* plots revealed co-expression of the neuropetides *Gal* > *Adcyap1* > *Bdnf* and *Cartpt* in Alk^{+} neurons. Moreover, many Alk^{+} neurons contained mRNAs for growth hormone receptor (*Ghr*), μ opioid receptors (*Oprm1*), opioid-related nociception receptor 1 (*Oprl1*), and ciliary neurotrophic factors (*Cntfr*) (Figure S6E). Finally, we assessed differential gene expression of glutamatergic and GABAergic markers and known constituents of the ALK signaling pathway in the five defined neuronal populations of the PVN: in pneSS neurons, we find expression (defined as >25% of cells/cluster) of *Slc17a6* (*Vglut2*); *Slc2a3* (*Glut3*); *Alk, Ptprz1* (regulator of ALK activity) (Perez-Pinera et al., 2007); *Jak2*, *Stat5b*, and *Ptn* (ALK ligand); and *Lmo4* (transcriptional repressor of *Alk*) (Lasek et al., 2011b) (Figure S6F). Expression of *Alk* in excitatory $Vglut2^{+}$ neurons was confirmed in an independent single-cell dataset from the hypothalamus (not shown).

Next, we searched to further annotate the thinness-associated *ALK* variants using public data from the University of California, Santa Cruz (UCSC) epigenomic web browser, as well as PhenoScanner and different brain eQTL (expression quantitative trait loci) databases. Chromatin state annotation predicted that the region is within an enhancer site in adipocytes and neurospheres (https://epigenomegateway.wustl.edu/) (Li et al., 2019). We cloned a 239 base pair fragment spanning the rs568057364 indel into a luciferase reporter vector (Muerdter et al., 2018) and introduced this reporter into SH-SY5Y neuroblastoma cells, which directly confirmed that this region has enhancer activity (Figure S6G). We also attempted to model both *ALK* indels in cell lines but the complexity (stretches of DNA with guanine/cytosine content >80%) and repetitiveness of the DNA sequence spanning the 2 *ALK* indels did not allow synthesis or targeting of the locus using CRISPR-Cas9. Therefore, we could not assess whether different variants affect enhancer activity. Taking advantage of the Human Brain Almanac, we investigated possible eQTL effects in 10 different brain regions. Owing to the modest sample size (n = 134 subjects), and in order to increase statistical power, we performed a set-based analyses of 11 SNPs (corresponding to SNPs with r-square >50% with our top variants). We found an eQTL effect with a false discovery rate (FDR) of 10% for three brain tissues, namely the temporal cortex, putamen, and cerebellar cortex (Table S4). Of note, we have no access to such data from the hypothalamus. Thus, in mouse and man, ALK is expressed in defined brain regions and the human variants appear to associate with altered expression.

Finally, to genetically map the tissue responsible for the observed action of *Alk* in thinness, we crossed our *Alk*-floxed mice to various tissue-specific Cre mouse lines. In line with our *Alk* expression data (Figure S5A), tissue-specific depletion of *Alk* in WAT (*AdipoqCre*) or BAT (*Ucp1Cre*), intestine (*VillinCre*), liver (*AlbuminCre*), muscle (*MckCre*), or hematopoietic cells (*Vav1-iCre*) did not affect HFD-induced obesity (Figures S7A–S7F). Of note, we could not analyze $Alk^{fl/fl}$ *NestinCre* mice, because our *NestinCre* line itself exhibits a strong metabolic phenotype, obscuring any conclusions (not shown). Because *Alk* is mainly expressed in the PVN, we therefore used stereotactic brain injections of adenovirus to target the PVN of $Alk^{fl/fl}$ mice and specifically deplete *Alk* expression. This approach also allowed us to exclude any potential developmental effects of *Alk* deletion. Control mice received an injection of the AAV::GFP viral vector ($Alk^{fl/fl}$ GFP), whereas the experimental group was co-injected with AAV::DIO-GFP (Cre-dependent GFP) and AAV::Cre

(H) Quantification of plasma adiponectin levels ($n \geq 15$).
(I) Body weight curves of male $Alk^{+/+}$ and $Alk^{-/-}$ mice housed at thermoneutrality ($n \geq 5$).
In (A–I), data are presented as mean ± SEM; *p < 0.05, **p < 0.01, ***p < 0.001, ****p < 0.0001; Student's two-tailed, unpaired t test (B, C, F, and H), Mann-Whitney U test (D), analysis of covariance (ANCOVA) using body weight as covariate (E), or two-way ANOVA followed by Bonferroni's multiple comparisons test (A, G, and I). See also Figure S3 and Table S3.

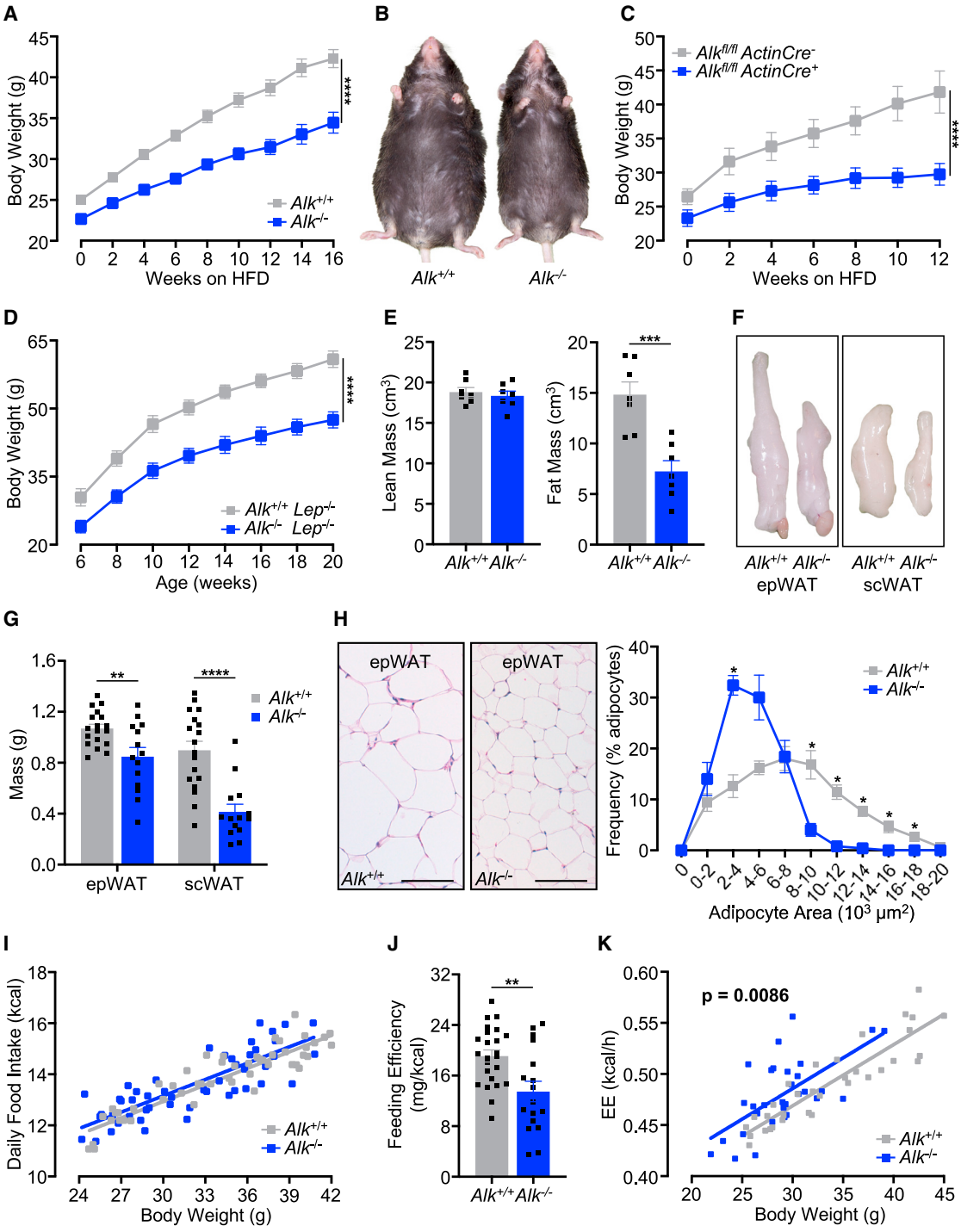

Figure 4. Genetic Deletion of *Alk* Increases Energy Expenditure and Confers Resistance to Diet- and Leptin-Mutation-Induced Obesity

(A and B) Body weight curves (A) and representative pictures (B) of $Alk^{+/+}$ and $Alk^{-/-}$ mice fed a HFD (n ≥ 23).

(C) Body weight curve of $Alk^{fl/fl}ActinCre^{-}$ and $Alk^{fl/fl}ActinCre^{+}$ mice fed a HFD (n ≥ 5).

(D) Body weight curves of SD-fed $Alk^{+/+}$ and $Alk^{-/-}$ mice on a leptin mutant ($Lep^{-/-}$) genetic background (n ≥ 6).

(E) Lean and fat mass of HFD fed mice measured by MRI (n = 7; 5 months old; 1 month on HFD).

(F and G) Representative pictures (F) and quantification (G) of epWAT and scWAT of HFD fed mice (n ≥ 14).

(H) Representative pictures of hematoxylin- and eosin-stained adipose tissue sections (left panels) and analysis of adipocyte cell size (right panels) of epWAT (n = 5; 16 weeks on HFD). Scale bar: 100 µm.

(legend continued on next page)

viral vectors ($Alk^{fl/fl}$ GFP+CRE), leading to PVN-specific deletion of *Alk* (Figure 5E). Following surgery, the mice recovered for 2 weeks and were subsequently fed a HFD. Strikingly, $Alk^{fl/fl}$ GFP+CRE mice showed resistance to HFD-induced obesity and reduced feeding efficiency relative to $Alk^{fl/fl}$ GFP mice (Figures 5F and 5G). These data show that ALK acts in the central nervous system to control body weight and weight gain.

Alk-Deficient Mice Exhibit Increased White Adipose Tissue Lipolysis

How does ALK in the PVN control fat metabolism? Plasma levels of PVN-regulated hormones corticosterone, thyroid-stimulating hormone (TSH) and oxytocin appeared normal in *Alk* mutant mice (Figures S7G–S7I). The PVN has also been shown to regulate sympathetic outflow to WAT (Bamshad et al., 1998; Foster et al., 2010) and BAT (Bamshad et al., 1999; Oldfield et al., 2002; Sved et al., 2001). Importantly, quantification of the sympathetic mediator norepinephrine (NE) in epWAT and scWAT revealed increased levels of NE in *Alk*-deficient mice compared to controls (Figure 6A), suggesting that *Alk* acts in the hypothalamus to control sympathetic tone to the fat tissue. We next asked whether increased sympathetic tone to the adipose tissue also exists in constitutionally thin humans. We took advantage of the availability of fat tissue samples from a previously described clinical study on 30 well-characterized constitutionally thin individuals (Ling et al., 2019). Paralleling our findings in mice, we indeed found markedly increased NE levels in the WAT of constitutionally thin subjects compared to their age- and sex-matched controls (Figure 6B).

Because NE induces lipolysis in fat tissues (Bartness et al., 2014), we focused on lipid storage and metabolism. As with mice on SD, HFD-fed $Alk^{+/+}$ and $Alk^{-/-}$ mice displayed normal levels of neutral sterols and bile acid content in the feces and plasma triglycerides (Figures S8A and S8B). Interestingly, despite reduced body adiposity, plasma non-esterified fatty acids (NEFA) levels were elevated in both male and female SD-fed $Alk^{-/-}$ mice (Figures S8C and S8D), our second $Alk^{-/-}$ mouse line $Alk^{fl/fl}$ $ActinCre^{+}$ (Figure S8E), and HFD-fed $Alk^{-/-}$ mice (Figure S8F) when compared to littermate controls. Moreover, adipose tissue NEFA levels were also increased in HFD-fed $Alk^{-/-}$ mice (Figure 6C), suggesting that $Alk^{-/-}$ mice exhibit increased adipose tissue lipolysis. To directly test this hypothesis, we measured phosphorylation of hormone sensitive lipase (HSL) at serine 660, a critical step in the induction of lipolysis (Holm, 2003). Indeed, western blot analysis revealed increased phosphorylation of HSL in both epWAT and scWAT of fasted $Alk^{-/-}$ mice fed SDs as well as HFDs compared to controls (Figures 6D and 6E). In line with increased HSL phosphorylation, we observed marked upregulation of seven key genes involved in fatty acid oxidation (*Pgc1α*, *Pdk4*, *Acox1*, *Cpt1b*, *Acads*, *Acadl*, and *Acadm*) in the epWAT of $Alk^{-/-}$ mice compared to $Alk^{+/+}$ mice fed SD (Figure 6F) as well as HFD (Figure 6G). We also observed enhanced NE levels and HSL-serine 660 phosphorylation in BAT of $Alk^{-/-}$ mice (Figures S8G and S8H). In addition, PVN-specific *Alk* depletion using stereotactic injections phenocopied the increased WAT lipolysis, as determined by HSL phosphorylation (Figure 6H).

NE has also been shown to induce browning of fat tissue (Harms and Seale, 2013). Whereas Ucp1 protein levels were apparently not changed in the BAT of *Alk* mutant mice (Figure S8H), we did observe increased levels of Ucp1 protein (Figure 6I) as well upregulation of thermogenic (*Elovl3*, *Cidea*, *Dio2*) and mitochondrial (*Pdk4*, *Acadl*, *Acadm*, *Cox7a*, *and Cox8b*) gene expression (Figure S8I) in the subcutaneous adipose tissue, indicating browning of WAT. Of note, increased levels of plasma NEFA levels and lipolysis did not result in ectopic fat deposition because liver and muscle triglyceride levels were not changed in HFD-fed mice (Figure S8J). Moreover, levels of inflammatory cytokines (IL-1β, IL-6, IL-10, iNOS, and TNF-α) were not changed in the liver of HFD-fed $Alk^{-/-}$ mice (Figure S8K). Overall, our data show that ALK in the PVN acts as a negative regulator of WAT lipolysis and sympathetic tone to fine-tune energy homeostasis.

DISCUSSION

Our results identify genetic variants in *ALK* associated with thinness as well as other metabolic traits in human. As the genetic association of the *ALK* variants with thinness remained correlative, we further characterized the metabolic function of ALK *in vivo*. A role for ALK in thinness was confirmed in *Drosophila* and multiple genetic mouse models, establishing a critical role for ALK in the regulation of thinness throughout evolution.

Few studies have evaluated the genetics of thinness. This is partly due to the difficulty of identifying suitable large cohorts in which the true metabolically healthy thinness state can be refined. We took advantage of the wide age range of the unique Estonian biobank recruitment as well as its strong phenotypic datasets, making ECGUT an ideal starting point to identify potential variants and genes playing a role in thinness. Of note, the Estonian population has been shown to be comparable to other European populations, in contrast to specific isolated populations such as Finns or Icelanders (Khrunin et al., 2013; Saag et al., 2019). Using the Estonian biobank, we identified multiple novel variants associated with thinness. These variants were further prioritized using fly genetic studies. This assumes that the allele with preliminary evidence for association with thinness in humans is the one that leads to either decreased expression or function of its target gene. In the case that the thinness allele would lead to increased expression or a gain of function with respect to the reference allele, the RNAi screen would miss those candidates. From the genes that showed an association

(I) Daily HFD intake of single-caged $Alk^{+/+}$ and $Alk^{-/-}$ mice ($n \geq 20$; 1 to 7 data points per mouse).
(J) Feeding efficiency on HFD (mg body weight gain per kcal consumed; $n \geq 17$; 1st month on HFD).
(K) Analysis of energy expenditure (EE) of HFD fed $Alk^{+/+}$ and $Alk^{-/-}$ mice using indirect calorimetry ($n \geq 31$).
In all panels, data are presented as mean ± SEM; *p < 0.05, **p < 0.01, ***p < 0.001, ****p < 0.0001; Student's two-tailed, unpaired t test (E, G, and J), Mann-Whitney U test (H), two-way ANOVA followed by Bonferroni's multiple comparisons test (A, C, and D), or ANCOVA using body weight as covariate (I and K). See also Figure S4.

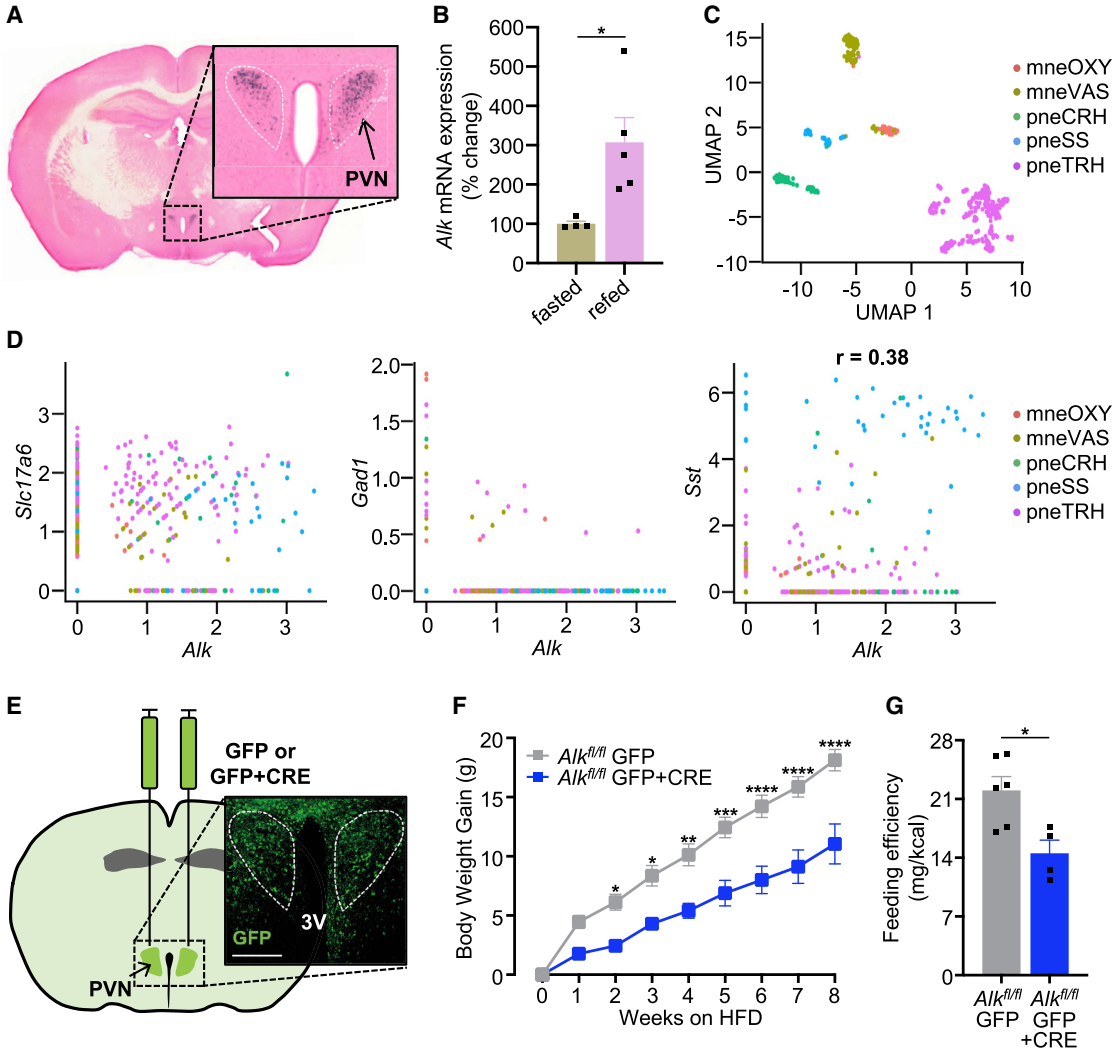

Figure 5. *Alk* Acts in the Central Nervous System

(A) Hypothalamic area serial sections of an $Alk^{-/-}$ mouse were stained for LacZ and counterstained with nuclear fast red.

(B) Hypothalamic mRNA expression of *Alk* in fasted and refed state of C57Bl6/J mice ($n \geq 4$).

(C) Separation of 514 PVN neurons into magnocellular neuroendocrine oxytocin (mneOXY), magnocellular neuroendocrine vasopressin (mneVAS), parvicellular neuroendocrine corticotropin-releasing hormone (pneCRH), parvicellular neuroendocrine somatostatin (pneSS), and parvicellular neuroendocrine thyrotropin-releasing hormone (pneTRH) neurons visualized by uniform manifold approximation and projection (UMAP) algorithm.

(D) Scatterplots showing co-expression of *Alk* and *Slc17a6* (*solute carrier family 17, member 6*; left panel), *Gad1* (*glutamate decarboxylase 1*; middle panel), or *Sst* (*somatostatin*; right panel) in the 5 neuronal populations of the PVN.

(E) Schematic diagram of stereotactic intracerebral injections of AAV::GFP (GFP) or AAV::DIO-GFP and AAV::Cre viral vectors (GFP+CRE) into $Alk^{fl/fl}$ mice targeting the PVN. Inset shows exemplary AVV infection (GFP signal in green). 3V, third ventricle. White lines mark the PVN. Scale bar: 200 μm.

(F) Body weight curves of $Alk^{fl/fl}$ GFP and $Alk^{fl/fl}$ GFP+CRE mice on HFD ($n \geq 4$).

(G) Feeding efficiency of $Alk^{fl/fl}$ GFP and $Alk^{fl/fl}$ GFP+CRE mice on HFD (mg body weight gain per kcal consumed; $n \geq 4$; first 3 weeks on HFD).

Data are presented as mean ± SEM; *p < 0.05, **p < 0.01, ***p < 0.001, ****p < 0.0001; Student's two-tailed, unpaired t test (B and G), Pearson's r correlation coefficient (D), or two-way ANOVA followed by Bonferroni's multiple comparisons test (F). See also Figures S5 and S6 and Tables S4 and S5.

with triglyceride levels in our fly screening assays, only for the *ALK* gene, the BMI-associated variants were located within the body of the gene. Importantly, in addition to the top *ALK* variants from the EGCUT cohort (indels rs568057364 and rs202021741), mining of GWAS data uncovered a further four downstream variants (rs12990552, rs10495771, rs55737023, and rs7578465) within the *ALK* locus that are associated with BMI in the GIANT (Fox et al., 2007; Locke et al., 2015) and UKBB (Yengo et al., 2018b) (http://www.nealelab.is/uk-biobank/) datasets. Conditional analyses with these four variants showed no impact on the association of the two *ALK* indels identified in our EGCUT GWAS with the thinness phenotype (rs568057364 p = 1.52E-06 and rs202021741 p = 4.71E-06), thereby demonstrating the independence of our *ALK* indels

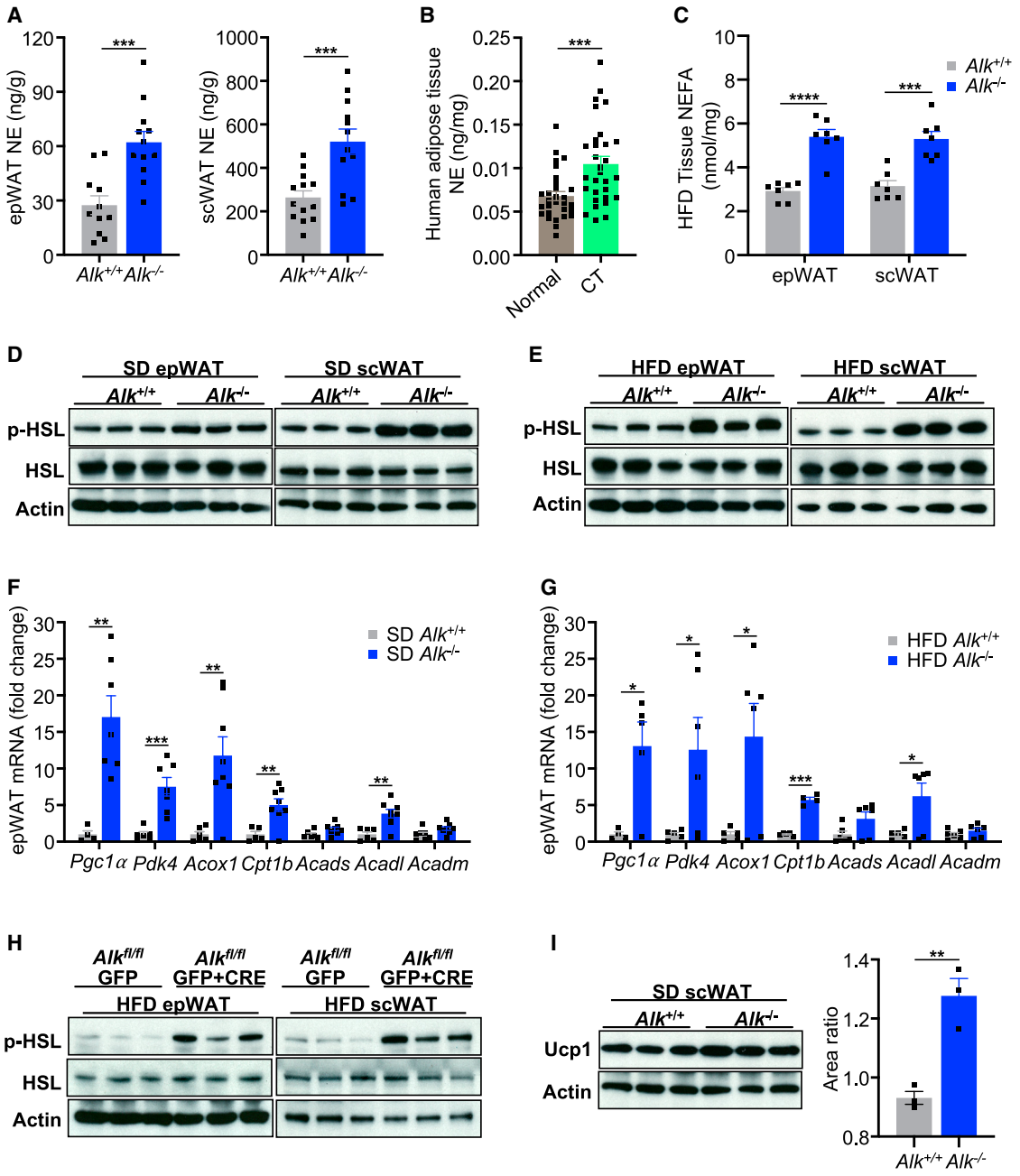

Figure 6. *Alk*-Deficient Mice Exhibit Increased White Adipose Tissue Lipolysis

(A) Quantification of norepinephrine (NE) in epWAT and scWAT of SD fed mice (n ≥ 11).

(B) Quantification of NE levels in white adipose tissue of constitutionally thin (CT) subjects compared to their age- and sex-matched controls (n ≥ 29).

(C) Quantification of adipose tissue non-esterified fatty acids (NEFA) levels in HFD-fed *Alk* knockout and littermate control mice (n = 7).

(D and E) Immunoblots for phosphorylated hormone-sensitive lipase (p-HSL), total HSL and, as loading control, Actin on epWAT and scWAT of SD- (D) and HFD-fed (E) mice.

(F and G) Quantification of fatty acid oxidation gene expression in the epWAT of SD- (F) and HFD-fed (G) $Alk^{+/+}$ and $Alk^{-/-}$ mice. mRNA levels of target genes were normalized to *36B4* expression, and data are presented as fold change to $Alk^{+/+}$. Abbreviations: *Pgc1α*, *peroxisome proliferator-activated receptor γ coactivator*; *Pdk4*, *pyruvate dehydrogenase kinase 4*; *Acox1*, *peroxisomal acyl-coenzyme A oxidase1*; *Cpt1b*, *carnitine palmitoyltransferase 1b*; *Acads*, *acyl-CoA dehydrogenase short chain*; *Acadl*, *acyl-CoA dehydrogenase long chain*; and *Acadm*, *acyl-CoA dehydrogenase medium chain*.

(H) Immunoblots for p-HSL, total HSL, and Actin on epWAT and scWAT of $Alk^{fl/fl}$ GFP and $Alk^{fl/fl}$ GFP+CRE mice on HFD.

(I) Immunoblots for Ucp1 and Actin on scWAT of SD-fed mice and densitometric quantification of western blot bands.

Data are presented as mean ± SEM; *p < 0.05, **p < 0.01, ***p < 0.001, ****p < 0.0001; Student's two-tailed, unpaired t test (A–C, F, G, and I). See also Figure S8.

and the BMI-associated *ALK* variants. Moreover, other variants within the *ALK* gene are associated with other metabolic traits, including adiponectin levels, glucose- and lipid homeostasis (Kathiresan et al., 2009; Lettre et al., 2011; Li et al., 2015; Meigs et al., 2007; Palmer et al., 2015). Thus, our ECGUT results and mining of GWAS data showed that several variants within the *ALK* locus are associated with metabolic traits such as lipid and glucose homeostasis, BMI, and, importantly, thinness.

In an attempt to replicate our human GWAS findings, we explored different cohorts. Importantly, our top two *ALK* variants are imputed indels and thus might not be systematically present in all cohorts (e.g., in GIANT studies). Moreover, they are located in a recombination hotspot and in low LD with other variants, making its detection challenging. In addition, the selection criteria for the UK Biobank (UKBB) (Sudlow et al., 2015) and STILTS (Study Into Lean and Thin Subjects) cohorts (Riveros-McKay et al., 2019) are different from the EGCUT cohort. First, the UKBB only includes individuals in the age range from 37 to 69, which is substantially older than the population selected in our study (20 to 44 years old). By selecting only the overlapping age categories (up to 45 years old) and using a similar BMI percentile approach as for the EGCUT analysis, the thinness-associating *ALK* variants identified in the EGCUT cohort were tested but did not associate with thinness in the UKBB. Second, the recent thinness study using the STILTS database (Riveros-McKay et al., 2019) identified persistently thin healthy individuals using a fixed BMI cutoff of less than 19, independent of age and gender. Moreover, less stringent selection criteria were used for the control group from the UK Household Longitudinal Study (UKHLS), whose BMI ranged from normal to obese (mean BMI 27 kg/m^2 +/− 8 SD), differed significantly in gender proportion (82% thin versus 55% control women, Fisher's exact test $p < 0.001$) and were significantly older than the thin subjects (52 versus 37 years old, t test $p < 0.001$). The UKBB is one of the largest and most commonly used prospective cohorts, yet, relative to the EGCUT cohort, targeted toward older age, where BMI associations become more variable. Indeed, using the full EGCUT cohort, we found a strong non-linear association between BMI and age (p value < 2e-16). When repeating such association analysis in subjects in the 20- to 45-year age category only, this complex relationship was still observed (p value = 0.016), yet it was significantly smaller (20-fold factor). Even though we did not observe a significant interaction between age and genotype effect (p values > 0.1 for both *ALK* indels) in our study, body composition changes are known to occur frequently in healthy people from the ages of 45–50 onward related to hormonal changes (such as menopause) and decreased physical activity (Davis et al., 2012; Guo et al., 1999). Our study is not empowered to evaluate a hormonal interaction with the genetic makeup in subjects above 46 years, but we used this upper age limit to exclude another factor of variability. We conclude that the different age distribution in the UKBB might be one factor contributing to the lack of replication.

The consequence of the intronic *ALK* variants associated with thinness requires further investigation. Our data suggest that the top *ALK* variants might be located in a regulatory region. Indeed, experimental enhancer assays in a human neuroblastoma cell line support the notion that at least the region around rs568057364 has enhancer activity. Moreover, eQTL analysis using the Brain Almanac data showed evidence for the *ALK* variants to affect ALK expression in specific brain regions, such as the cerebellar cortex, putamen, and temporal cortex: brain regions in which *ALK* expression was among the highest. Yet at this stage we cannot pinpoint any direct causal effect of the variants on *ALK* expression in humans because this would require access to both hypothalamus-specific gene expression data and also large sample size to perform reliable Mendelian randomization analyses (Burgess, 2014; Davies et al., 2018). A direct link between the *ALK* variants and human thinness is therefore preliminary and requires additional validation in other cohorts and follow-up studies.

Nonetheless, although all these data are supporting the notion of ALK being involved in metabolism in human, the caveats of GWAS have been demonstrated in case of the most prominent obesity associated gene, *FTO*. Although several studies showed that intronic variants of the *FTO* gene robustly associate with human obesity (Dina et al., 2007; Frayling et al., 2007; Scuteri et al., 2007), follow-up studies revealed that two neighboring genes, *IRX3* and *RPGRIP1L*, rather than *FTO* activity itself, are responsible for the observed body weight effects (Tung et al., 2014). Therefore, it was paramount to directly demonstrate that ALK is indeed involved in weight regulation and glucose homeostasis. Our mouse knockouts of *Alk*, using two distinct and independently generated mutant lines, results in thin mice at normal diet, HFD, and under conditions of leptin deficiency. These genetic data provide direct proof that ALK has a role in weight regulation, with striking similarities to the human thinness phenotype.

Our data in *Drosophila* show that Alk downregulations using RNAi results in reduced triglyceride levels. Moreover, we previously identified Alk as a hit for "skinny" *Drosophila* in our genome-wide screen for obesity (Pospisilik et al., 2010) and another fly study identified Alk as a cell-intrinsic regulator of organ sparing (neuroblasts) under conditions of nutrient restriction (Cheng et al., 2011). Because our mechanistic mouse data now show that ALK slows lipolysis and maintains adipose storage, anabolic and catabolic lipid flux and excess fat storage might be evolutionary conserved to ensure protection from cold and regulate nutrient availability.

Unlike patients with anorexia nervosa, a disease tightly linked to psychiatric phenotypes (Duncan et al., 2017), metabolically healthy thin individuals often have the desire to gain weight and have normal food intake and frequently snack, indicating they have a metabolic rather than hedonic low body weight. The metabolic body weight set point has a genetic basis, programmed by the energy balance circuitry in the hypothalamus and other specific brain regions (Yu et al., 2015). A recent clinical study led by some of the authors of our study showed that thin individuals (with BMI lower than 18.5 kg/m^2) have a distinct adipose-specific molecular signature, with smaller adipocytes, increased adipose mitochondrial activity, and concomitant augmented fatty acid oxidation, similar to the phenotypes of *Alk* mutant mice. Furthermore, plasma proteomic analyses demonstrated significantly higher plasma levels of dopamine beta-hydroxylase (DBH) in thin individuals (23% higher), which was speculated to be an indicator for an increased sympathetic neuro-adipose axis in thin subjects (Ling et al., 2019).

Importantly, we now report enhanced levels of NE in the adipose tissue of constitutively thin humans. In addition, we found increased NE levels in the white as well as brown fat of *Alk* mutant mice, providing genetic evidence that *Alk* deficiency is associated with an altered sympathetic tone to the adipose organ. In line with enhanced sympathetic activation, we found molecular evidence for increased lipolysis as well as browning of the fat tissue, ultimately resulting in reduced feeding efficiency and enhanced EE independent of circadian activity, which mechanistically explains why *Alk* mutant mice remain thin.

Expression analysis revealed high *Alk* mRNA levels in the hypothalamus, especially in the PVN, which is also true for humans. Single-cell RNA sequencing in mouse showed that *Alk* is primarily expressed in the pneSS population within the PVN, in excitatory neurons in particular. Importantly our functional knockout data show that *Alk* expression in the PVN is indeed the critical site for the observed resistance to weight gain under HFD. The PVN receives inputs from several hypothalamic nuclei including the arcuate nucleus and the lateral hypothalamus and regulates energy homeostasis via hormonal pathways and the sympathetic nervous system (Hill, 2012). Interestingly, our single-cell profiling also showed that *Alk*-expressing neurons in the PVN overlap with *Lmo4* expression. LMO4 (LIM domain only 4) was reported to repress *Alk* transcription (Lasek et al., 2011b) and ablation of LMO4 in mouse excitatory glutamatergic neurons, including neurons of the PVN, results in obesity, reduced energy expenditure, and reduced sympathetic outflow to adipose tissue (Zhou et al., 2012), further strengthening the notion that *Alk* is part of a brain circuit that controls feeding efficiency and EE. How ALK-expressing neurons shape metabolic control and how loss of ALK activity can ultimately overcome an obesogenic environment needs further investigation.

Leptin mediates its lipolytic effect through the action of sympathetic nerve fibers that innervate the adipose tissue (Zeng et al., 2015). Our data that inactivation of *Alk* results in increased sympathetic tone to adipose tissue and markedly reduces obesity in leptin mutant mice also suggest a crosstalk to other key neuronal paths that control body mass (Yi et al., 2013). Therefore, ALK pathway inhibition might promote thinness even in leptin resistance and other conditions of general and morbid obesity (Sáinz et al., 2015), highlighting the therapeutic potential of ALK inhibition. ALK has gained prominence in cancer as a key oncogenic driver and as a drug target in multiple tumors. However, although ALK is a member of the insulin-receptor superfamily (Morris et al., 1994), its physiological function was largely unknown. Our human GWAS data along with genetic and functional studies in flies and mice place ALK as a key central nervous system regulator of EE and identify *ALK* as a candidate gene for thinness.

STAR★METHODS

Detailed methods are provided in the online version of this paper and include the following:

SUPPLEMENTAL INFORMATION

Supplemental Information can be found online at https://doi.org/10.1016/j.cell.2020.04.034.

ACKNOWLEDGMENTS

We would like to thank all members of our laboratories for constructive critiques and expert advice. Furthermore, we acknowledge Life Science Editors for editorial support and the IMP-IMBA graphics department for support on illustrations. We thank Alexander Stark for help with designing the enhancer assay. We are grateful to the Biomedical Sequencing Facility at the CeMM Research Center for Molecular Medicine of the Austrian Academy of Sciences for assistance with next-generation sequencing and G.A. Bazykin for providing access to the 2TB RAM "Makarich" computational cluster for OMICS data analysis. We also thank Jeremy Schwartzentruber for feedback on annotation of the variants and Solenn Pruvost from the Nestlé genomics core for help with sequencing. This work was supported by the Estonian Research Council (IUT20-60), European Union Horizon 2020 (692145), and European Union through the European Regional Development Fund (2014-2020.4.01.15-0012 GENTRANSMED). Q.-P.W. was supported by the Natural Science Foundation of Guangdong Province (no. 2018B030306002) and Natural Science Foundation of China (no. 31800993). E.O.T. is supported by a Ph.D. fellowship from the Austrian Science Fund (FWF) (DOC 33-B27), and T.H. is supported by the Swedish Research Council (Vetenskapsrådet; grants 2013-3080 and 2018-02838), the Swedish Brain Foundation (Hjärnfonden; grants FO2017-0293 and FO2019-0277), and the European Research Council (SECRET-CELLS, 2015-AdG-695136). W.H. was supported by a grant from the European Community's Seventh Framework Programme (FP/2007-2013)/ERC grant agreement no. 311701), the Research Institute of Molecular Pathology (IMP), Boehringer Ingelheim, and the Austrian Research Promotion Agency (FFG). J.M.P. is supported by grants from IMBA, the Austrian Academy of Sciences, the T. von Zastrow Foundation, the FWF Wittgenstein award (Z 271-B19), and a C150 grant from the Canadian government.

AUTHOR CONTRIBUTIONS

J.M.P. and M.O. designed and supervised the mouse study. J.H., N.G., and A.V. designed the GWAS, selected population groups, and interpreted GWAS results. A.M. provided access to EGCUT biobank data. A.V. supervised and contributed to EGCUT GWAS analysis, with help from R.M. and M. Nõukas. R.M. and M.L. performed UKBB analysis. Q.-P.W. and T.C. performed fly experiments with supervision from G.G.N. M.O. performed mouse experiments. S.M. performed speed congenics analysis. J.K. performed mouse

stereotaxic surgery with supervision from W.H. I.K. performed western blot experiments. M.T. and K.S. performed quantitative PCR with supervision from A.H. and F.W.K. A.J. performed measurements of adipocyte size and S.A. performed analysis of *Alk* expression using the mouse tissue library with supervision from H.E. V.K., L.M.Z., and J.L. performed analysis of lean and fat mass (MRI), U.J.F.T. performed feces analysis, and I.T. performed analysis of intestinal absorption. M.O., A.L., D.C., C.N., and C.A. performed enhancer assay. E.O.T., Z.D., C.-C.H., and T.H. performed single-cell RNA-seq analysis. E.D., R.H., and A.B. performed triglyceride and NEFA measurements and qPCR of liver inflammatory markers. S.J.F.C. performed hot plate assay experiments. M. Novatchkova, J.A.P., and V.N. contributed to study design and scientific discussions. M.O., N.G., and J.M.P. wrote the paper with input from the co-authors.

DECLARATION OF INTERESTS

J.H., N.G., and A.V. are employed by Nestlé Research. J.H., N.G., and A.V. have filed a patent on Methods of Modulating ALK (WO2019101490).

Received: April 28, 2019
Revised: January 28, 2020
Accepted: April 20, 2020
Published: May 21, 2020

REFERENCES

Abarca-Gómez, L., Abdeen, Z.A., Hamid, Z.A., Abu-Rmeileh, N.M., Acosta-Cazares, B., Acuin, C., Adams, R.J., Aekplakorn, W., Afsana, K., Aguilar-Salinas, C.A., et al.; NCD Risk Factor Collaboration (NCD-RisC) (2017). Worldwide trends in body-mass index, underweight, overweight, and obesity from 1975 to 2016: a pooled analysis of 2416 population-based measurement studies in 128·9 million children, adolescents, and adults. Lancet *390*, 2627–2642.

Abecasis, G.R., Auton, A., Brooks, L.D., DePristo, M.A., Durbin, R.M., Handsaker, R.E., Kang, H.M., Marth, G.T., McVean, G.A., Gabriel, S.B., et al.; 1000 Genomes Project Consortium (2012). An integrated map of genetic variation from 1,092 human genomes. Nature *491*, 56–65.

Apfelbaum, M., and Sachet, P. (1982). [Constitutional thinness]. Rev. Prat. *32*, 245–247.

Auton, A., Brooks, L.D., Durbin, R.M., Garrison, E.P., Kang, H.M., Korbel, J.O., Marchini, J.L., McCarthy, S., McVean, G.A., and Abecasis, G.R.; 1000 Genomes Project Consortium (2015). A global reference for human genetic variation. Nature *526*, 68–74.

Bamshad, M., Aoki, V.T., Adkison, M.G., Warren, W.S., and Bartness, T.J. (1998). Central nervous system origins of the sympathetic nervous system outflow to white adipose tissue. Am. J. Physiol. *275*, R291–R299.

Bamshad, M., Song, C.K., and Bartness, T.J. (1999). CNS origins of the sympathetic nervous system outflow to brown adipose tissue. Am. J. Physiol. *276*, R1569–R1578.

Bartness, T.J., Liu, Y., Shrestha, Y.B., and Ryu, V. (2014). Neural innervation of white adipose tissue and the control of lipolysis. Front. Neuroendocrinol. *35*, 473–493.

Becares, N., Gage, M.C., Voisin, M., Shrestha, E., Martin-Gutierrez, L., Liang, N., Louie, R., Pourcet, B., Pello, O.M., Luong, T.V., et al. (2019). Impaired LXRα Phosphorylation Attenuates Progression of Fatty Liver Disease. Cell Rep. *26*, 984–995.e6.

Bilsland, J.G., Wheeldon, A., Mead, A., Znamenskiy, P., Almond, S., Waters, K.A., Thakur, M., Beaumont, V., Bonnert, T.P., Heavens, R., et al. (2008). Behavioral and neurochemical alterations in mice deficient in anaplastic lymphoma kinase suggest therapeutic potential for psychiatric indications. Neuropsychopharmacology *33*, 685–700.

Bulik, C.M., and Allison, D.B. (2001). The genetic epidemiology of thinness. Obes. Rev. *2*, 107–115.

Burgess, S. (2014). Sample size and power calculations in Mendelian randomization with a single instrumental variable and a binary outcome. Int. J. Epidemiol. *43*, 922–929.

Caron, A., Labbé, S.M., Lanfray, D., Blanchard, P.G., Villot, R., Roy, C., Sabatini, D.M., Richard, D., and Laplante, M. (2015). Mediobasal hypothalamic overexpression of DEPTOR protects against high-fat diet-induced obesity. Mol. Metab. *5*, 102–112.

Cheng, L.Y., Bailey, A.P., Leevers, S.J., Ragan, T.J., Driscoll, P.C., and Gould, A.P. (2011). Anaplastic lymphoma kinase spares organ growth during nutrient restriction in Drosophila. Cell *146*, 435–447.

Conway, J.R., Lex, A., and Gehlenborg, N. (2017). UpSetR: an R package for the visualization of intersecting sets and their properties. Bioinformatics *33*, 2938–2940.

Cowley, M.A., Pronchuk, N., Fan, W., Dinulescu, D.M., Colmers, W.F., and Cone, R.D. (1999). Integration of NPY, AGRP, and melanocortin signals in the hypothalamic paraventricular nucleus: evidence of a cellular basis for the adipostat. Neuron *24*, 155–163.

Davies, N.M., Holmes, M.V., and Davey Smith, G. (2018). Reading Mendelian randomisation studies: a guide, glossary, and checklist for clinicians. BMJ *362*, k601.

Davis, S.R., Castelo-Branco, C., Chedraui, P., Lumsden, M.A., Nappi, R.E., Shah, D., and Villaseca, P.; Writing Group of the International Menopause Society for World Menopause Day 2012 (2012). Understanding weight gain at menopause. Climacteric *15*, 419–429.

Delaneau, O., Marchini, J., and Zagury, J.F. (2011). A linear complexity phasing method for thousands of genomes. Nat. Methods *9*, 179–181.

Della Corte, C.M., Viscardi, G., Di Liello, R., Fasano, M., Martinelli, E., Troiani, T., Ciardiello, F., and Morgillo, F. (2018). Role and targeting of anaplastic lymphoma kinase in cancer. Mol. Cancer *17*, 30.

Dina, C., Meyre, D., Gallina, S., Durand, E., Körner, A., Jacobson, P., Carlsson, L.M.S., Kiess, W., Vatin, V., Lecoeur, C., et al. (2007). Variation in FTO contributes to childhood obesity and severe adult obesity. Nat. Genet. *39*, 724–726.

Duncan, L., Yilmaz, Z., Gaspar, H., Walters, R., Goldstein, J., Anttila, V., Bulik-Sullivan, B., Ripke, S., Thornton, L., Hinney, A., et al.; Eating Disorders Working Group of the Psychiatric Genomics Consortium (2017). Significant Locus and Metabolic Genetic Correlations Revealed in Genome-Wide Association Study of Anorexia Nervosa. Am. J. Psychiatry *174*, 850–858.

Durinck, S., Spellman, P.T., Birney, E., and Huber, W. (2009). Mapping identifiers for the integration of genomic datasets with the R/Bioconductor package biomaRt. Nat. Protoc. *4*, 1184–1191.

el Marjou, F., Janssen, K.P., Chang, B.H.J., Li, M., Hindie, V., Chan, L., Louvard, D., Chambon, P., Metzger, D., and Robine, S. (2004). Tissue-specific and inducible Cre-mediated recombination in the gut epithelium. Genesis *39*, 186–193.

Estour, B., Galusca, B., and Germain, N. (2014). Constitutional thinness and anorexia nervosa: a possible misdiagnosis? Front. Endocrinol. (Lausanne) *5*, 175.

Fischer, A.W., Cannon, B., and Nedergaard, J. (2018). Optimal housing temperatures for mice to mimic the thermal environment of humans: An experimental study. Mol. Metab. *7*, 161–170.

Folch, J., Lees, M., and Sloane Stanley, G.H. (1957). A simple method for the isolation and purification of total lipides from animal tissues. J. Biol. Chem. *226*, 497–509.

Foster, M.T., Song, C.K., and Bartness, T.J. (2010). Hypothalamic paraventricular nucleus lesion involvement in the sympathetic control of lipid mobilization. Obesity (Silver Spring) *18*, 682–689.

Fox, C.S., Heard-Costa, N., Cupples, L.A., Dupuis, J., Vasan, R.S., and Atwood, L.D. (2007). Genome-wide association to body mass index and waist circumference: the Framingham Heart Study 100K project. BMC Med. Genet. *8* (*Suppl 1*), S18.

Frayling, T.M., Timpson, N.J., Weedon, M.N., Zeggini, E., Freathy, R.M., Lindgren, C.M., Perry, J.R.B., Elliott, K.S., Lango, H., Rayner, N.W., et al. (2007). A common variant in the FTO gene is associated with body mass index and predisposes to childhood and adult obesity. Science *316*, 889–894.

Germain, N., Galusca, B., Caron-Dorval, D., Martin, J.F., Pujos-Guillot, E., Boirie, Y., Khalfallah, Y., Ling, Y., Minnion, J.S., Bloom, S.R., et al. (2014).

Specific appetite, energetic and metabolomics responses to fat overfeeding in resistant-to-bodyweight-gain constitutional thinness. Nutr. Diabetes *4*, e126.

Goldstein, J.I., Crenshaw, A., Carey, J., Grant, G.B., Maguire, J., Fromer, M., O'Dushlaine, C., Moran, J.L., Chambert, K., Stevens, C., et al.; Swedish Schizophrenia Consortium; ARRA Autism Sequencing Consortium (2012). zCall: a rare variant caller for array-based genotyping: genetics and population analysis. Bioinformatics *28*, 2543–2545.

Guan, J., Umapathy, G., Yamazaki, Y., Wolfstetter, G., Mendoza, P., Pfeifer, K., Mohammed, A., Hugosson, F., Zhang, H., Hsu, A.W., et al. (2015). FAM150A and FAM150B are activating ligands for anaplastic lymphoma kinase. eLife *4*, e09811.

Guo, S.S., Zeller, C., Chumlea, W.C., and Siervogel, R.M. (1999). Aging, body composition, and lifestyle: the Fels Longitudinal Study. Am. J. Clin. Nutr. *70*, 405–411.

Hafemeister, C., and Satija, R. (2019). Normalization and variance stabilization of single-cell RNA-seq data using regularized negative binomial regression. Genome Biol. *20*, 296.

Hallberg, B., and Palmer, R.H. (2016). The role of the ALK receptor in cancer biology. Ann. Oncol. *27* (*Suppl 3*), iii4–iii15.

Harms, M., and Seale, P. (2013). Brown and beige fat: development, function and therapeutic potential. Nat. Med. *19*, 1252–1263.

Hill, J.W. (2012). PVN pathways controlling energy homeostasis. Indian J. Endocrinol. Metab. *16* (*Suppl 3*), S627–S636.

Holm, C. (2003). Molecular mechanisms regulating hormone-sensitive lipase and lipolysis. Biochem. Soc. Trans. *31*, 1120–1124.

Horvat, S., Bünger, L., Falconer, V.M., Mackay, P., Law, A., Bulfield, G., and Keightley, P.D. (2000). Mapping of obesity QTLs in a cross between mouse lines divergently selected on fat content. Mamm. Genome *11*, 2–7.

Howie, B.N., Donnelly, P., and Marchini, J. (2009). A flexible and accurate genotype imputation method for the next generation of genome-wide association studies. PLoS Genet. *5*, e1000529.

Huckins, L.M., Dobbyn, A., Ruderfer, D.M., Hoffman, G., Wang, W., Pardiñas, A.F., Rajagopal, V.M., Als, T.D.T., Nguyen, H., Girdhar, K., et al. (2019). Gene expression imputation across multiple brain regions provides insights into schizophrenia risk. Nat. Genet. *51*, 659–674.

Huszar, D., Lynch, C.A., Fairchild-Huntress, V., Dunmore, J.H., Fang, Q., Berkemeier, L.R., Gu, W., Kesterson, R.A., Boston, B.A., Cone, R.D., et al. (1997). Targeted disruption of the melanocortin-4 receptor results in obesity in mice. Cell *88*, 131–141.

Iwahara, T., Fujimoto, J., Wen, D., Cupples, R., Bucay, N., Arakawa, T., Mori, S., Ratzkin, B., and Yamamoto, T. (1997). Molecular characterization of ALK, a receptor tyrosine kinase expressed specifically in the nervous system. Oncogene *14*, 439–449.

Ja, W.W., Carvalho, G.B., Mak, E.M., De La Rosa, N.N., Fang, A.Y., Liong, J.C., Brummel, T., and Benzer, S. (2007). Prandiology of *Drosophila* and the CAFE assay. Proc. Natl. Acad. Sci. U S A *104*, 8253–8256.

Kamat, M.A., Blackshaw, J.A., Young, R., Surendran, P., Burgess, S., Danesh, J., Butterworth, A.S., and Staley, J.R. (2019). PhenoScanner V2: an expanded tool for searching human genotype-phenotype associations. Bioinformatics *35*, 4851–4853.

Kathiresan, S., Willer, C.J., Peloso, G.M., Demissie, S., Musunuru, K., Schadt, E.E., Kaplan, L., Bennett, D., Li, Y., Tanaka, T., et al. (2009). Common variants at 30 loci contribute to polygenic dyslipidemia. Nat. Genet. *41*, 56–65.

Khrunin, A.V., Khokhrin, D.V., Filippova, I.N., Esko, T., Nelis, M., Bebyakova, N.A., Bolotova, N.L., Klovins, J., Nikitina-Zake, L., Rehnström, K., et al. (2013). A genome-wide analysis of populations from European Russia reveals a new pole of genetic diversity in northern Europe. PLoS ONE *8*, e58552.

Laplante, M., Horvat, S., Festuccia, W.T., Birsoy, K., Prevorsek, Z., Efeyan, A., and Sabatini, D.M. (2012). DEPTOR cell-autonomously promotes adipogenesis, and its expression is associated with obesity. Cell Metab. *16*, 202–212.

Lasek, A.W., Lim, J., Kliethermes, C.L., Berger, K.H., Joslyn, G., Brush, G., Xue, L., Robertson, M., Moore, M.S., Vranizan, K., et al. (2011a). An evolutionary conserved role for anaplastic lymphoma kinase in behavioral responses to ethanol. PLoS ONE *6*, e22636.

Lasek, A.W., Gesch, J., Giorgetti, F., Kharazia, V., and Heberlein, U. (2011b). Alk is a transcriptional target of LMO4 and ERα that promotes cocaine sensitization and reward. J. Neurosci. *31*, 14134–14141.

Laskarzewski, P.M., Khoury, P., Morrison, J.A., Kelly, K., Mellies, M.J., and Glueck, C.J. (1983). Familial obesity and leanness. Int. J. Obes. *7*, 505–527.

Lettre, G., Palmer, C.D., Young, T., Ejebe, K.G., Allayee, H., Benjamin, E.J., Bennett, F., Bowden, D.W., Chakravarti, A., Dreisbach, A., et al. (2011). Genome-wide association study of coronary heart disease and its risk factors in 8,090 African Americans: the NHLBI CARe Project. PLoS Genet. *7*, e1001300.

Li, M.X., Gui, H.S., Kwan, J.S.H., and Sham, P.C. (2011). GATES: a rapid and powerful gene-based association test using extended Simes procedure. Am. J. Hum. Genet. *88*, 283–293.

Li, W.D., Jiao, H., Wang, K., Yang, F., Grant, S.F.A., Hakonarson, H., Ahima, R., and Arlen Price, R. (2015). Pathway-based genome-wide association studies reveal that the Rac1 pathway is associated with plasma adiponectin levels. Sci. Rep. *5*, 13422.

Li, D., Hsu, S., Purushotham, D., Sears, R.L., and Wang, T. (2019). WashU Epigenome Browser update 2019. Nucleic Acids Res *47*, W158–W165.

Ling, Y., Carayol, J., Galusca, B., Canto, C., Montaurier, C., Matone, A., Vassallo, I., Minehira, K., Alexandre, V., Cominetti, O., et al. (2019). Persistent low body weight in humans is associated with higher mitochondrial activity in white adipose tissue. Am. J. Clin. Nutr. *110*, 605–616.

Locke, A.E., Kahali, B., Berndt, S.I., Justice, A.E., Pers, T.H., Day, F.R., Powell, C., Vedantam, S., Buchkovich, M.L., Yang, J., et al.; LifeLines Cohort Study; ADIPOGen Consortium; AGEN-BMI Working Group; CARDIOGRAMplusC4D Consortium; CKDGen Consortium; GLGC; ICBP; MAGIC Investigators; MuTHER Consortium; MIGen Consortium; PAGE Consortium; ReproGen Consortium; GENIE Consortium; International Endogene Consortium (2015). Genetic studies of body mass index yield new insights for obesity biology. Nature *518*, 197–206.

Loh, P.-R., Kichaev, G., Gazal, S., Schoech, A.P., and Price, A.L. (2018). Mixed-model association for biobank-scale datasets. Nat. Genet. *50*, 906–908.

Lorén, C.E., Scully, A., Grabbe, C., Edeen, P.T., Thomas, J., McKeown, M., Hunter, T., and Palmer, R.H. (2001). Identification and characterization of DAlk: a novel Drosophila melanogaster RTK which drives ERK activation in vivo. Genes Cells *6*, 531–544.

Lotta, L.A., Mokrosiński, J., Mendes de Oliveira, E., Li, C., Sharp, S.J., Luan, J., Brouwers, B., Ayinampudi, V., Bowker, N., Kerrison, N., et al. (2019). Human Gain-of-Function MC4R Variants Show Signaling Bias and Protect against Obesity. Cell *177*, 597–607.e9.

Lu, Y., Day, F.R., Gustafsson, S., Buchkovich, M.L., Na, J., Bataille, V., Cousminer, D.L., Dastani, Z., Drong, A.W., Esko, T., et al. (2016). New loci for body fat percentage reveal link between adiposity and cardiometabolic disease risk. Nat. Commun. *7*, 10495.

Machiela, M.J., and Chanock, S.J. (2015). LDlink: a web-based application for exploring population-specific haplotype structure and linking correlated alleles of possible functional variants. Bioinformatics *31*, 3555–3557.

Maes, H.H.M., Neale, M.C., and Eaves, L.J. (1997). Genetic and environmental factors in relative body weight and human adiposity. Behav. Genet. *27*, 325–351.

Magnusson, P.K.E., and Rasmussen, F. (2002). Familial resemblance of body mass index and familial risk of high and low body mass index. A study of young men in Sweden. Int. J. Obes. Relat. Metab. Disord. *26*, 1225–1231.

Mangieri, R.A., Maier, E.Y., Buske, T.R., Lasek, A.W., and Morrisett, R.A. (2017). Anaplastic lymphoma kinase is a regulator of alcohol consumption and excitatory synaptic plasticity in the nucleus accumbens shell. Front. Pharmacol. *8*, 533.

Marchini, J., Howie, B., Myers, S., McVean, G., and Donnelly, P. (2007). A new multipoint method for genome-wide association studies by imputation of genotypes. Nat. Genet. *39*, 906–913.

McInnes, L., Healy, J., Saul, N., and Großberger, L. (2018). UMAP: Uniform Manifold Approximation and Projection (J. Open Source Softw).

Meigs, J.B., Manning, A.K., Fox, C.S., Florez, J.C., Liu, C., Cupples, L.A., and Dupuis, J. (2007). Genome-wide association with diabetes-related traits in the Framingham Heart Study. BMC Med. Genet. *8* (*Suppl 1*), S16.

Morris, S.W., Kirstein, M.N., Valentine, M.B., Dittmer, K.G., Shapiro, D.N., Saltman, D.L., and Look, A.T. (1994). Fusion of a kinase gene, ALK, to a nucleolar protein gene, NPM, in non- Hodgkin's lymphoma. Science *263*, 1281–1284.

Morton, N.M., Densmore, V., Wamil, M., Ramage, L., Nichol, K., Bünger, L., Seckl, J.R., and Kenyon, C.J. (2005). A polygenic model of the metabolic syndrome with reduced circulating and intra-adipose glucocorticoid action. Diabetes *54*, 3371–3378.

Muerdter, F., Boryń, Ł.M., Woodfin, A.R., Neumayr, C., Rath, M., Zabidi, M.A., Pagani, M., Haberle, V., Kazmar, T., Catarino, R.R., et al. (2018). Resolving systematic errors in widely used enhancer activity assays in human cells. Nat. Methods *15*, 141–149.

Murray, P.B., Lax, I., Reshetnyak, A., Ligon, G.F., Lillquist, J.S., Natoli, E.J., Jr., Shi, X., Folta-Stogniew, E., Gunel, M., Alvarado, D., and Schlessinger, J. (2015). Heparin is an activating ligand of the orphan receptor tyrosine kinase ALK. Sci. Signal. *8*, ra6.

Oldfield, B.J., Giles, M.E., Watson, A., Anderson, C., Colvill, L.M., and McKinley, M.J. (2002). The neurochemical characterisation of hypothalamic pathways projecting polysynaptically to brown adipose tissue in the rat. Neuroscience *110*, 515–526.

Palmer, N.D., Goodarzi, M.O., Langefeld, C.D., Wang, N., Guo, X., Taylor, K.D., Fingerlin, T.E., Norris, J.M., Buchanan, T.A., Xiang, A.H., et al. (2015). Genetic variants associated with quantitative glucose homeostasis traits translate to type 2 diabetes in Mexican Americans: The GUARDIAN (Genetics underlying diabetes in Hispanics) consortium. Diabetes *64*, 1853–1866.

Pan, W., Kim, J., Zhang, Y., Shen, X., and Wei, P. (2014). A powerful and adaptive association test for rare variants. Genetics *197*, 1081–1095.

Paxinos, G., and Franklin, K.B.J. (2007). The mouse brain in stereotaxic coordinates (Elsevier Science).

Perez-Pinera, P., Zhang, W., Chang, Y., Vega, J.A., and Deuel, T.F. (2007). Anaplastic lymphoma kinase is activated through the pleiotrophin/receptor protein-tyrosine phosphatase β/ζ signaling pathway: an alternative mechanism of receptor tyrosine kinase activation. J. Biol. Chem. *282*, 28683–28690.

Pospisilik, J.A., Schramek, D., Schnidar, H., Cronin, S.J.F., Nehme, N.T., Zhang, X., Knauf, C., Cani, P.D., Aumayr, K., Todoric, J., et al. (2010). Drosophila genome-wide obesity screen reveals hedgehog as a determinant of brown versus white adipose cell fate. Cell *140*, 148–160.

Purcell, S., Neale, B., Todd-Brown, K., Thomas, L., Ferreira, M.A.R., Bender, D., Maller, J., Sklar, P., de Bakker, P.I.W., Daly, M.J., and Sham, P.C. (2007). PLINK: a tool set for whole-genome association and population-based linkage analyses. Am. J. Hum. Genet. *81*, 559–575.

Ran, S., Zhang, L., Liu, L., Feng, A.P., Pei, Y.F., Zhang, L., Han, Y.Y., Lin, Y., Li, X., Kong, W.W., et al. (2017). Gene-based genome-wide association study identified 19p13.3 for lean body mass. Sci. Rep. *7*, 45025.

Ren, D., Zhou, Y., Morris, D., Li, M., Li, Z., and Rui, L. (2007). Neuronal SH2B1 is essential for controlling energy and glucose homeostasis. J. Clin. Invest. *117*, 397–406.

Riveros-McKay, F., Mistry, V., Bounds, R., Hendricks, A., Keogh, J.M., Thomas, H., Henning, E., Corbin, L.J., O'Rahilly, S., Zeggini, E., et al.; Understanding Society Scientific Group (2019). Genetic architecture of human thinness compared to severe obesity. PLoS Genet. *15*, e1007603.

Romanov, R.A., Zeisel, A., Bakker, J., Girach, F., Hellysaz, A., Tomer, R., Alpár, A., Mulder, J., Clotman, F., Keimpema, E., et al. (2017). Molecular interrogation of hypothalamic organization reveals distinct dopamine neuronal subtypes. Nat. Neurosci. *20*, 176–188.

Saag, L., Laneman, M., Varul, L., Malve, M., Valk, H., Razzak, M.A., Shirobokov, I.G., Khartanovich, V.I., Mikhaylova, E.R., Kushniarevich, A., et al. (2019). The Arrival of Siberian Ancestry Connecting the Eastern Baltic to Uralic Speakers further East. Curr. Biol. *29*, 1701–1711.e16.

Sáinz, N., Barrenetxe, J., Moreno-Aliaga, M.J., and Martínez, J.A. (2015). Leptin resistance and diet-induced obesity: central and peripheral actions of leptin. Metabolism *64*, 35–46.

Scopelliti, A., Bauer, C., Yu, Y., Zhang, T., Kruspig, B., Murphy, D.J., Vidal, M., Maddocks, O.D.K., and Cordero, J.B. (2019). A Neuronal Relay Mediates a Nutrient Responsive Gut/Fat Body Axis Regulating Energy Homeostasis in Adult Drosophila. Cell Metab. *29*, 269–284.e10.

Scuteri, A., Sanna, S., Chen, W.M., Uda, M., Albai, G., Strait, J., Najjar, S., Nagaraja, R., Orrú, M., Usala, G., et al. (2007). Genome-wide association scan shows genetic variants in the FTO gene are associated with obesity-related traits. PLoS Genet. *3*, e115.

Shabalin, A.A. (2012). Matrix eQTL: ultra fast eQTL analysis via large matrix operations. Bioinformatics *28*, 1353–1358.

Simmons, D.M., and Swanson, L.W. (2009). Comparison of the spatial distribution of seven types of neuroendocrine neurons in the rat paraventricular nucleus: toward a global 3D model. J. Comp. Neurol. *516*, 423–441.

Staley, J.R., Blackshaw, J., Kamat, M.A., Ellis, S., Surendran, P., Sun, B.B., Paul, D.S., Freitag, D., Burgess, S., Danesh, J., et al. (2016). PhenoScanner: a database of human genotype-phenotype associations. Bioinformatics *32*, 3207–3209.

Stoica, G.E., Kuo, A., Aigner, A., Sunitha, I., Souttou, B., Malerczyk, C., Caughey, D.J., Wen, D., Karavanov, A., Riegel, A.T., and Wellstein, A. (2001). Identification of anaplastic lymphoma kinase as a receptor for the growth factor pleiotrophin. J. Biol. Chem. *276*, 16772–16779.

Stoica, G.E., Kuo, A., Powers, C., Bowden, E.T., Sale, E.B., Riegel, A.T., and Wellstein, A. (2002). Midkine binds to anaplastic lymphoma kinase (ALK) and acts as a growth factor for different cell types. J. Biol. Chem. *277*, 35990–35998.

Stuart, T., Butler, A., Hoffman, P., Hafemeister, C., Papalexi, E., Mauck, W.M., 3rd, Hao, Y., Stoeckius, M., Smibert, P., and Satija, R. (2019). Comprehensive Integration of Single-Cell Data. Cell *177*, 1888–1902.e21.

Sudlow, C., Gallacher, J., Allen, N., Beral, V., Burton, P., Danesh, J., Downey, P., Elliott, P., Green, J., Landray, M., et al. (2015). UK biobank: an open access resource for identifying the causes of a wide range of complex diseases of middle and old age. PLoS Med. *12*, e1001779.

Sved, A.F., Cano, G., and Card, J.P. (2001). Neuroanatomical specificity of the circuits controlling sympathetic outflow to different targets. Clin. Exp. Pharmacol. Physiol. *28*, 115–119.

Tschöp, M.H., Speakman, J.R., Arch, J.R.S., Auwerx, J., Brüning, J.C., Chan, L., Eckel, R.H., Farese, R.V., Jr., Galgani, J.E., Hambly, C., et al. (2011). A guide to analysis of mouse energy metabolism. Nat. Methods *9*, 57–63.

Tung, Y.C.L., Yeo, G.S.H., O'Rahilly, S., and Coll, A.P. (2014). Obesity and FTO: Changing focus at a complex locus. Cell Metab. *20*, 710–718.

Turpin, S.M., Nicholls, H.T., Willmes, D.M., Mourier, A., Brodesser, S., Wunderlich, C.M., Mauer, J., Xu, E., Hammerschmidt, P., Brönneke, H.S., et al. (2014). Obesity-induced CerS6-dependent C16:0 ceramide production promotes weight gain and glucose intolerance. Cell Metab. *20*, 678–686.

van Buuren, S., and Groothuis-Oudshoorn, K. (2011). mice: Multivariate imputation by chained equations in R. J. Stat. Softw. https://doi.org/10.18637/jss.v045.i03.

Vernersson, E., Khoo, N.K.S., Henriksson, M.L., Roos, G., Palmer, R.H., and Hallberg, B. (2006). Characterization of the expression of the ALK receptor tyrosine kinase in mice. Gene Expr. Patterns *6*, 448–461.

Wakeland, E., Morel, L., Achey, K., Yui, M., and Longmate, J. (1997). Speed congenics: a classic technique in the fast lane (relatively speaking). Immunol. Today *18*, 472–477.

Weiss, J.B., Xue, C., Benice, T., Xue, L., Morris, S.W., and Raber, J. (2012). Anaplastic lymphoma kinase and leukocyte tyrosine kinase: functions and

genetic interactions in learning, memory and adult neurogenesis. Pharmacol. Biochem. Behav. *100*, 566–574.

Williams, G., Bing, C., Cai, X.J., Harrold, J.A., King, P.J., and Liu, X.H. (2001). The hypothalamus and the control of energy homeostasis: different circuits, different purposes. Physiol. Behav. *74*, 683–701.

Yaswen, L., Diehl, N., Brennan, M.B., and Hochgeschwender, U. (1999). Obesity in the mouse model of pro-opiomelanocortin deficiency responds to peripheral melanocortin. Nat. Med. *5*, 1066–1070.

Yengo, L., Sidorenko, J., Kemper, K.E., Zheng, Z., Wood, A.R., Weedon, M.N., Frayling, T.M., Hirschhorn, J., Yang, J., Visscher, P.M., et al. (2018a). Meta-analysis of genome-wide association studies for height and body mass index in ~700,000 individuals of European ancestry. bioRxiv. https://doi.org/10.1101/274654.

Yengo, L., Sidorenko, J., Kemper, K.E., Zheng, Z., Wood, A.R., Weedon, M.N., Frayling, T.M., Hirschhorn, J., Yang, J., and Visscher, P.M.; GIANT Consortium (2018b). Meta-analysis of genome-wide association studies for height and body mass index in :700000 individuals of European ancestry. Hum. Mol. Genet. *27*, 3641–3649.

Yi, C.X., Meyer, C.W., and Jastroch, M. (2013). Leptin action in the brain: How (and when) it makes fat burn. Mol. Metab. *2*, 63–64.

Yu, Y.H., Vasselli, J.R., Zhang, Y., Mechanick, J.I., Korner, J., and Peterli, R. (2015). Metabolic vs. hedonic obesity: a conceptual distinction and its clinical implications. Obes. Rev. *16*, 234–247.

Zeng, W., Pirzgalska, R.M., Pereira, M.M.A., Kubasova, N., Barateiro, A., Seixas, E., Lu, Y.H., Kozlova, A., Voss, H., Martins, G.G., et al. (2015). Sympathetic neuro-adipose connections mediate leptin-driven lipolysis. Cell *163*, 84–94.

Zhou, X., Gomez-Smith, M., Qin, Z., Duquette, P.M., Cardenas-Blanco, A., Rai, P.S., Harper, M.E., Tsai, E.C., Anisman, H., and Chen, H.H. (2012). Ablation of LMO4 in glutamatergic neurons impairs leptin control of fat metabolism. Cell. Mol. Life Sci. *69*, 819–828.

Zillikens, M.C., Demissie, S., Hsu, Y.-H., Yerges-Armstrong, L.M., Chou, W.-C., Stolk, L., Livshits, G., Broer, L., Johnson, T., Koller, D.L., et al. (2017). Large meta-analysis of genome-wide association studies identifies five loci for lean body mass. Nat. Commun. *8*, 80.

STAR★METHODS

KEY RESOURCES TABLE

REAGENT or RESOURCE	SOURCE	IDENTIFIER
Antibodies		
Mouse monoclonal anti-β-actin	Sigma	A5316; RRID: AB_476743
Rabbit polyclonal anti-HSL	Cell Signaling	4107; RRID: AB_2296900
Rabbit polyclonal anti-phospho-HSL (Ser660)	Cell Signaling	4126; RRID: AB_490997
Rabbit polyclonal anti-Ucp1	Abcam	ab10983; RRID: AB_2241462
Goat polyclonal anti-mouse IgG HRP	Promega	W4021; RRID: AB_430834
Rabbit IgG HRP linked F(ab')2	GE Healthcare	NA9340V; RRID: AB_772191
Biological Samples		
Human adipose tissue samples	Nestlé	Ling et al., 2019
Chemicals, Peptides, and Recombinant Proteins		
3H-triolein	PerkinElmer	NET431001MC
Tyloxapol	Sigma Aldrich	T8761
Ultima Gold	Perkin Elmer	6013119
Petroleum ether 60-80	Supelco	1.01774
BSTFA	Supelco	15222
TMCS	Supelco	1.02333
Heptane	Supelco	1.04390
Sep-Pak C18	Waters	WAT054945
Phosphoblocker Blocking Rgnt	Cell Biolabs	AKR-103
ECL Plus	Pierce	1896327
TRIzol	Invitrogen	15596018
RIPA buffer	Sigma	R0278
Halt protease and phosphatase inhibitor cocktail	Thermo Scientific	78440
DNase inactivation reagent	Ambion	#AM1906
dt18	NEB	#S1316S
dNTPs	NEB	#4475
RNase Inhibitor	Thermo Fisher	#EN0531
DTT	Invitrogen	#18080093 within SSIII kit
Strand buffer	Invitrogen	#18080093 within SSIII kit
Critical Commercial Assays		
Mouse Ultrasensitive Insulin ELISA	Alpco	80-INSMSU-E10
Triglycerides, GPO-PAP	Dialab	D00390
HR Series NEFA-HR (2)	Wako	991-34891
Corticosterone ELISA kit	Enzo Life Sciences	ADI-900-097
Mouse thyrotropin subunit beta ELISA	EIAAB	E0463m
Mouse adiponectin/Acrp30 Immunoassay	Quantikine	MRP300
Oxytocin ELISA kit	Enzo Life Sciences	ADI-900-153A
PeqGold TriFast	VWR	30-2010
M-MLV Reverse Transcriptase	Thermo Scientific	28025021
Universal Probes Mastermix	BioRad	172-5284
RevertAid RT Kit	Thermo Scientific	K1691
DNase I, RNase-free	Thermo Scientific	EN0521
FastStart Universal SYBR Green Master	Roche	04913914001
QIAshredder	QIAGEN	#79654

(*Continued on next page*)

Continued

REAGENT or RESOURCE	SOURCE	IDENTIFIER
RNeasy mini prep kit	QIAGEN	#74104
TurboDNase	Invitrogen	#AM2238
Superscript III	Invitrogen	#18080093
SybrGreen	Thermo Fisher	#4309155
Free Fatty Acid Assay Kit	Abcam	Ab65341
Triglycerides for Cobas Integra	Roche Diagnostics	#20767107322
Deposited Data		
GWAS thin-versus-control	This manuscript	http://www.geenivaramu.ee/tools/THIN_NORMAL_FILTER_MAF_1prc_INFO_0.8.txt.gz
GWAS control-versus-obese	This manuscript	http://www.geenivaramu.ee/tools/OBESE_NORMAL_FILTER_MAF_1prc_INFO_0.8.txt.gz
Human genotype data	This manuscript	https://genomics.ut.ee/en/biobank.ee/data-access
Single cell RNaseq	Gene Expression Omnibus	GSE132730
Experimental Models: Cell Lines		
ES cells: $Alk^{tm1a(EUCOMM)Wtsi}$	EUCOMM	EPD0632_2_E02
SH-SY5Y	Sigma	94030304
Experimental Models: Organisms/Strains		
D. melanogaster: Act-Gal4/cyo	Bloomington	BDSC:4414
D. melanogaster: eIF2B-b RNAi	VDRC	VDRC:25426
D. melanogaster: CG11052 RNAi	VDRC	VDRC:23373
D. melanogaster: CG42675 RNAi	VDRC	VDRC:16171
D. melanogaster: CG33346 RNAi	VDRC	VDRC:47842
D. melanogaster: Syn1 RNAi	VDRC	VDRC:27893
D. melanogaster: Hth RNAi	VDRC	VDRC:12764
D. melanogaster: Spred RNAi	VDRC	VDRC:18024
D. melanogaster: Alk RNAi	VDRC	VDRC:107083
D. melanogaster: Paf-Aha RNAi	VDRC	VDRC:29003
D. melanogaster: AdamTS-A RNAi	VDRC	VDRC:33347
D. melanogaster: Nsun2 RNAi	VDRC	VDRC:37601
D. melanogaster: Trf4-2 RNAi	VDRC	VDRC:19799
D. melanogaster: Alk Overexpression	Ruth Palmer Lab	Lorén et al., 2001
Mouse: $Alk^{tm1Dgen}$ (B6/J)	Deltagen	T1477
Mouse: Mdk^{tm1Tmu}	RIKEN BRC animal	RBRC02422
Mouse: Ptn^{tm1Tmu}	RIKEN BRC animal	RBRC02411
Mouse: $Alk^{fl/fl}$	This manuscript	derived from $Alk^{tm1a(EUCOMM)Wtsi}$
Mouse: $Tg(Ucp1\text{-}icre)^{\#Jcbr}$	Jens Bruening Lab	Turpin et al., 2014
Mouse: FVB/N-*Tmem163*$^{Tg(ACTB\text{-}cre)2Mrt}$/J	Jackson Laboratory	Stock No 003376
Mouse: Villin cre	Sylvie Robine Lab	el Marjou et al., 2004
Mouse: B6.Cg-*Commd10*$^{Tg(Vav1\text{-}icre)A2Kio}$/J	Jackson Laboratory	Stock No 008610
Mouse: B6;FVB-Tg(Adipoq-cre)1Evdr/J	Jackson Laboratory	Stock No 010803
Mouse: B6.Cg-Speer6-ps1$^{Tg(Alb\text{-}cre)21Mgn}$/J	Jackson Laboratory	Stock No 003574
Mouse: B6.FVB(129S4)-Tg(Ckmm-cre)5Khn/J	Jackson Laboratory	Stock No 006475
Mouse: B6.Cg-*Lep*^{ob}/J	Jackson Laboratory	Stock No 000632
Mouse: C57BL/6J	Jackson Laboratory	Strain Code 632
Oligonucleotides		
See Table S6	This manuscript	N/A

(*Continued on next page*)

Continued

REAGENT or RESOURCE	SOURCE	IDENTIFIER
Recombinant DNA		
Luciferase reporter vector	Addgene	#99297
Negative control vector	Addgene	#99315
Renilla control vector	Promega	#E2261
Software and Algorithms		
GenomeStudio Software	Illumina	https://emea.support.illumina.com/array/array_software/genomestudio/downloads.html?langsel=/ch/
IMPUTE2	Marchini et al., 2007	http://mathgen.stats.ox.ac.uk/impute/impute_v2.html https://genome.sph.umich.edu/wiki/IMPUTE2:_1000_Genomes_Imputation_Cookbook
1000 Genomes Phase 3, b37, October 2014	Auton et al., 2015	https://mathgen.stats.ox.ac.uk/impute/1000GP%20Phase%203%20haplotypes%206%20October%202014.html
BOLT-LMM v2.3 software	Loh et al., 2018	https://data.broadinstitute.org/alkesgroup/BOLT-LMM/
R 3.4.4	The R Foundation	https://www.r-project.org/
Amira 6.0.0	This manuscript	https://www.thermofisher.com
AxioVision morphometry software	Zeiss	https://www.zeiss.at/mikroskopie/downloads.html
Fiji/ImageJ version v2.0	Fiji/ImageJ	https://imagej.net/Fiji/Downloads
GraphPad Prism 8.3.0	GraphPad	https://www.graphpad.com/scientific-software/prism/
biomaRt. Interface to BioMart databases (i.e., Ensembl). v2.42.0	Durinck et al., 2009	https://bioconductor.org/packages/biomaRt
Seurat. Tools for Single Cell Genomics. v3.1.1	Stuart et al., 2019	https://github.com/satijalab/seurat
scTransform. Variance Stabilizing Transformations for Single Cell UMI Data. v0.2.0	Hafemeister and Satija, 2019	https://github.com/ChristophH/sctransform
UpSetR. A More Scalable Alternative to Venn and Euler Diagrams for Visualizing Intersecting Sets. V1.4.0.	Conway et al., 2017	https://github.com/hms-dbmi/UpSetR
Plink	Purcell et al., 2007	https://www.cog-genomics.org/plink/1.9/
SNPTEST	Marchini et al., 2007	https://mathgen.stats.ox.ac.uk/genetics_software/snptest/snptest.html
MICE	van Buuren and Groothuis-Oudshoorn, 2011	https://cran.r-project.org/web/packages/mice
PhenoScanner	Kamat et al., 2019 Staley et al., 2016	http://www.phenoscanner.medschl.cam.ac.uk/
GATES (as implemented in aSPU R package)	Li et al., 2011	https://cran.r-project.org/web/packages/aSPU/index.html
LDlink	Machiela and Chanock, 2015	https://ldlink.nci.nih.gov/
Other		
Standard chow diet	ssniff	V1184-300
High fat diet	Research Diets	D12492i

RESOURCE AVAILABILITY

Lead Contact

Further information and requests for resources and reagents should be directed to and will be fulfilled by the Lead Contact, Josef M. Penninger (josef.penninger@ubc.ca).

Materials Availability

All mouse lines generated in this study are available upon request.

Data and Code Availability

GWAS summary stats are publicly available under the following links:

http://www.geenivaramu.ee/tools/THIN_NORMAL_FILTER_MAF_1prc_INFO_0.8.txt.gz

http://www.geenivaramu.ee/tools/OBESE_NORMAL_FILTER_MAF_1prc_INFO_0.8.txt.gz

The raw genotype data are available on demand and access to data can be requested under https://genomics.ut.ee/en/biobank.ee/data-access.

Single-cell RNA-seq were deposited in Gene Expression Omnibus (accession number: GSE132730).

EXPERIMENTAL MODELS AND SUBJECT DETAILS

Studies in humans

Individuals were selected from the EGCUT (Estonian Genomic Center of the University of Tartu) cohort (https://genomics.ut.ee/en). At the time of analysis, this population-based biobank contained clinical data and biological samples from 47102 individuals. All participants provided informed consent. The study was approved by the local ethics committees (Switzerland, protocol number 279/14).

Studies in flies

Fly stocks were maintained on standard diet with agar, sugar and yeast and were raised in 25°C incubator at a 12/12 dark and night cycle. Actin-Gal4 was from Bloomington. RNAi fly lines were from the VDRC (Vienna *Drosophila* Resource Center).

Studies in mice

Experimental animals were housed in SMI type2 long standard filtertop or individually ventilated cages, fed *ad libitum* and checked daily by veterinary staff. Unless stated otherwise, only male littermate mice group-housed at room temperature (~23°C) were used for all experiments described and randomly assigned to experimental groups. All animal experiments were approved by the Austrian Animal Care and Use Committee.

METHOD DETAILS

Studies in Humans

Population selection

The thinness phenotype was defined as those people with the lowest 6th percentile BMI in the cohort adjusted for age and sex. Age ranged from 20 to 44 years old. Strict exclusion criteria based on ICD10 codes (Table S1) were applied, including pregnancy, breastfeeding, postmenopausal or menstrual abnormalities, subjects with eating disorders according to DSMIV, severe chronic diseases (e.g., diabetes), professional athletes, depression or psychiatric condition (anti-depressant treatment), past surgery known to influence the endocrine system and/or weight (especially bariatric surgery), subjects under known treatment with beta-blockers, anti-hypertensives, lipid lowering drugs or corticoids for a long duration, as well as cancer patients. Control individuals were selected based on age-adjusted BMI in the 30-50th percentile, while obese individuals had a BMI in the highest 95th percentile of the population-wide BMI range (Figure S1). Using these criteria, 881 putative thinness individuals were identified (one third male and two third females), as well as 3173 age- and sex-matched controls, and 555 age- and sex-matched obese individuals.

Genotyping

Genotype data were generated using HumanCorePsy array (Illumina, San Diego, USA). Genotypes were called with the GenomeStudio Software (Illumina). Rare variant genotype calling was performed using zCall (Goldstein et al., 2012). Genotype quality control removed any subject with SNP call rate lower than 98%, any gender discrepancies between known gender and inferred gender from genotype data, genotype heterozygosity > 3 standard deviations, population outlier (as detected with MDS analyses). Quality control also excluded any marker if the call rate was lower than 95%, it deviated from Hardy-Weinberg equilibrium ($p < 1e\text{-}4$), was a rare variant with Minor Allele Frequency (MAF) lower than 1%, and A/T or C/G genotypes (prior imputation). Genotype imputation was performed using SHAPEIT (Delaneau et al., 2011) and IMPUTE2 (Howie et al., 2009) based reference panels from the 1000 Genomes project (Abecasis et al., 2012) (1000 Genomes integrated haplotypes, Dec 2013 release). Post-imputation quality control removed markers with INFO score < 0.8 or MAF < 1%. In total, the genotype data consisted of 281K genotyped and 8.3M imputed markers.

Studies in flies

Functional analyses of Drosophila *lines*

10 virgin *Actin-Gal4/CyO* virgin females were crossed with 5-7 young UAS-RNAi or control w1118 males to drive RNAi-mediated whole-body knockdown of target genes. Once the F1 flies hatched, males were selected and at the age of 4-7 days put onto normal diet (10% sucrose, 10% yeast) or high sucrose diet (47.5% sucrose, 10% yeast) for 10 days. Body weight was measured using an analytic balance. For triglyceride measurements, 10 male flies were weighted and homogenized in 200 μL PBST (PBS + 0.05% Tween

20) on ice and sonicated. After sonication, 800 μL ice-cold PBST was added and mixed thoroughly. 50 μL of the mixture was used to determine the triglycerides using the Roche triglycerides kit (11730711216) under the manufacturer's instructions. Triglyceride levels were normalized to body weight. The values were converted to a Z-score based on the following formula: ((Mean of Individual-Mean of Controls)/SD of control) and the cut off was at a 95% confidence interval on a 2-tailed test, which corresponded to a Z score of $\geq$ 1.96 or ≤ -1.96. Any target gene considered as a hit was confirmed by three independent screens for confirmation.

Food intake assay in Drosophila

Food intake was measured by CAFE assay, which was modified from a previous study (Ja et al., 2007). 5 male flies (4 days old) were put into each vial with wet paper at bottom and empty vials were used for evaporation controls. Liquid food of 5% yeast extract and 10% sucrose were loaded into 5 μl capillary and put into each vial for food intake assay. All food intake experiments were set up at Zeitgeber time 6–8, and food intake was recorded exactly 24 h after start of food loading.

Lifespan assay in Drosophila

For assessment of fly lifespan, 45 male flies were collected per genotype and the number of dead flies was counted every 2-3 days when flies were transferred to new medium.

Studies in mice

Mouse lines and diets

Mice were housed on a 14/10 h light/dark cycle (except for indirect calorimetry and thermoneutrality, where mice were on a 12/12 h light/dark cycle). Standard chow diet was purchased from SSNIFF (V 1184-300; 10mm pellets autoclavable; 49% kcal carbohydrates, 36% kcal protein and 15% kcal fat) and high fat diet from ResearchDiets (D12492i; 20% kcal carbohydrates, 20% kcal protein and 60% kcal fat). *Alk* conventional knockout mice, containing a LacZ cassette, were purchased from Deltagen (www.informatics.jax.org/allele/MGI:5700373); *Mdk* and *Ptn* knockout mice were both purchased from Riken BRC (https://www.brc.riken.jp/); $Alk^{flox/flox}$ conditional knockout mice were derived in-house from targeted ES cells generated by the European Conditional Mouse Mutagenesis Program (www.eucomm.org); *Ucp1* Cre mice were kindly provided by Dr. Jan-Wilhelm Kornfeld (Jens Bruening Lab); *β-Actin* Cre mice were kindly provided by Dr. Andreas Leibbrandt (originally Nasmyth group – IMP) and *Villin* Cre mice originate from Institut Curie (Sylvie Robine Lab). The following mouse lines were obtained from the Jackson Laboratory (https://www.jax.org/): *β-Actin* Cre (FVB/N-$Tmem163^{Tg(ACTB-cre)2Mrt}$/J); *Adipoq* Cre (B6;FVB-Tg(Adipoq-cre)1Evdr/J); *Alb* Cre (B6.Cg-Speer6-ps1Tg(Alb-cre)21Mgn/J); *Mck* Cre (B6.FVB(129S4)-Tg(Ckmm-cre)5Khn/J); *Vav1-i* Cre (B6.Cg-Commd10Tg(Vav1-icre)A2Kio/J) and *Lep* knockout mice (B6.Cg-Lepob/J).

Accelerated backcrossing of Alk *knockout mice to C57BL/6 genetic background*

An autosomal genome scan was performed by means of a low-density panel of 88 DNA-microsatellite markers (short tandem repeats, STRs) which show isogenic strain-specific allele fragment lengths (Wakeland et al., 1997). Map locations and primer sequences of the microsatellite loci were used according to the Mouse Locus List (http://www.informatics.jax.org). The PCR-based scan was applied to 40 backcrossed mice; the animals showing the highest percentage of recipient strain genome and the smallest size of the donor strain element co-segregating with the site of interest were used for further backcrossing.

Phenotypic analysis and histopathology

In difference to all other experiments, where *Alk* knockout mice were backcrossed to C57BL/6 using speed congenics, animals used for global phenotypic and behavioral analysis as well as histopathology were still on a mixed genetic background of C57BL/6 and 129.

Behavioral tests. All behavioral tests were performed on the same group of adult males 10-12 weeks ($n \geq 7$). Mice were run through the behavioral programs in the following order: open field test, tail flick test, rotarod test and hot plate test. Females were not studied due to variability caused by the estrous cycle. Males were group-housed, with no access to females post-weaning. Wild-type and homozygous mutant mice were not segregated by cage. Mice were allowed to habituate to the behavior room environment for 30 min prior to experimentation unless otherwise indicated. Chambers were sanitized with a 0.25% bleach solution before each test and between animals. The experimenters changed gloves before handling mice from different cages.

Mice were screened for behavioral abnormalities by evaluating the response to a novel environment using an open field test (ENV-515; constructed with opaque PVC, 43.2 × 43.2 × 30.5 cm; https://www.med-associates.com). Movement of animals was monitored by an array of 16 infrared detectors. The computer controller allowed the operation of 8 independent chambers simultaneously. Each animal was placed gently in the center of its assigned chamber. Tests were for 10 min, with the experimenter out of the animals' sight. Activity of individual mice was recorded for the 10-min test session and monitored by photobeam breaks in the x-, y- and z axes. Measurements taken include total distance traveled, percent of session time spent in the central region of the test apparatus and average velocity during the ambulatory episodes.

For the tail flick test, a high intensity light beam was directed at the restrained tail of the mouse through a small hole and latency to the tail flick was detected automatically. Inter-trial intervals lasted at least 60 s.

The Accelerating Rotarod (AccuScan Instruments, Inc.; Columbus, OH 43228) was used to screen for motor coordination, balance and ataxia phenotypes. The unit consists of an analyzer with 4 ports to connect up to 4 test chambers. Each test chamber is individually controlled. The analyzer is connected to a computer's serial COM port and interfaced via Windows 3.1 software. Light beams are used for sensing an animal's fall. Each test chamber records the time when the animal falls off the rotating rod (70 mm in diameter), and the speed of rod at the time of fall. Test chambers are fully enclosed, so the animals are not able to jump out or see neighboring

subjects. Mice were allowed to move about on their wire-cage top for 30 s prior to testing to ensure awareness. Mice were placed on the stationary rod, facing away from the experimenter. The ''speed profile'' programs the rotarod to reach 60 rpm after six minutes. Most mice fell from the rotarod between 30 and 90 s after the test is begun. A photobeam is broken when the animal falls, which stops the test clock for that chamber. The animals were tested over three trials with a 20-min rest period between trials.

For the hot plate assay, wild-type and mutant litter-mate mice were tested for hot plate latency at 50°C and 55°C (UGO Basile, Model 35100). Mice were placed gently on the surface and the time from then until response was noted. Responses include licking of either hind paw or jumping.

Physical exam. Male and female mice (age bin: 49 and 300 days) were first observed in their home cages for a number of general characteristics such as activity level, behavior toward siblings, posture, grooming, breathing pattern and sounds, and movement. General body condition and size were noted as well. Following a visual inspection of the mouse in the cage, the mouse was handled for a detailed, stepwise examination. The head was examined first, including eyes, ears, and nose, noting any discharge, malformations, or other abnormalities. Lymph nodes and glands of the head and neck were palpated. Skin, hair coat, axial and appendicular skeleton, and abdomen were also assessed. The limbs and torso were palpated for masses, malformations or other abnormalities. The anogenital region was examined for discharges, staining of hair, or other changes. If the mouse defecated during the examination, the feces were assessed for color and consistency.

Fertility. The reproductive traits of male (67-159 days old) and female *Alk* mutant mice were tested to identify potential defects in spermatogenesis, oogenesis, maternal ability to support pre- or post-embryonic development, or mammary gland defects and ability of the female knockout mice to nurse their pups. Three homozygous mutant mice of each gender were set up in a fertility mating with a homozygous mutant mouse of the opposite gender at seven to eight weeks of age. The numbers of pups born from one to three litters were recorded at birth. Three weeks later, the live pups were counted and weaned.

Necropsy. The necropsy, or post-mortem examination, was performed following deep general anesthesia, cardiac puncture for terminal blood collection, and euthanasia. The necropsy, which was done in a stepwise fashion, included detailed examination of the whole mouse, the skinned carcass, skeleton, and all major organ systems. Significant lesions and abnormal findings in organs and tissues were noted during the examination. When an organ appeared normal, the term ''NSA'' or ''No Significant Abnormalities'' was chosen. Terms such as mass, exudate, discoloration, and others were chosen as appropriate to describe changes in organs. Organs were fixed in 10% neutral buffered formalin and submitted to the histopathology laboratory for processing. Male and female mice (age bin: 49 and 300 days) were examined for the following observables: adrenal glands, bone marrow, bone - cranium, bone - femur, bone - sternum, bone - stifle joint, bone - vertebral column, brain, cecum, colon, duodenum, epididymis - seminal vesicle, esophagus, eyes, gallbladder, general appearance, harderian glands, heart, ileum, jejunum, kidneys, liver, lungs, lymph nodes, mesentery, ovaries, pancreas, penis, salivary glands, sciatic nerve, scrotum, skeletal muscle, skin, skinned mouse, spleen, stomach, testes, thymus, tongue, trachea, urinary bladder, urine, uterus, and vagina.

Histopathology. The following tissues of male and female mice (age bin: 49 and 300 days) were examined: white adipose tissue, brown adipose tissue, brain, pituitary gland, ears, nasal cavity, salivary glands, oral cavity, lymph nodes, aorta, lungs, liver, gallbladder, pancreas, spleen, kidneys, urinary bladder, stomach, small and large intestines, larynx, esophagus, trachea, thyroid gland, thymus gland, tongue, skeletal muscle, sciatic nerve, mammary glands, vertebrae, spinal cord, bone (skull, sternum, femur, tibia, and stifle joint), reproductive tract (including gonads), eyes, harderian glands, integumentary system (skin and either clitoral or preputial glands), and bone marrow (examined in sections of sternum, vertebrae, and/or femur and tibia).

Hematology. Blood samples of male and female mice (age bin: 49, 90, 180 and 300 days) were collected via a terminal cardiac puncture in a syringe. One hundred microliters of each whole blood sample were transferred into tubes pre-filled with EDTA. Approximately 25uL of the blood were placed onto a glass slide to prepare a peripheral blood smear. The blood smears were later stained with Wright's Stain that differentially stains white blood cell nuclei, granules and cytoplasm, and allows the identification of different cell types. The slides were analyzed microscopically by counting and noting each cell type in a total of 100 white blood cells. The percentage of each of the cell types counted was then calculated. Red blood cell morphology was also evaluated. Furthermore, whole blood was analyzed using a Cell-Dyn 3700 Hematology Analyzer. The following parameters were measured: white blood cells, red blood cells, red blood cell morphology, haemoglobin, hematocrit, platelets, mean corpuscular volume, mean corpuscular haemoglobin, mean corpuscular haemoglobin concentration, neutrophils, lymphocytes, monocytes, eosinophils and basophils.

Serum Chemistry. The following analytes were measured in male and female mice (age bin: 49, 90, 180 and 300 days): electrolytes (sodium, potassium, chloride, bicarbonate); renal function (blood urea nitrogen, creatinine, osmolality), inorganic ions (calcium, phosphorus), liver function (alkaline phosphatase, alanine aminotransferase, aspartate transferase, lactate dehydrogenase, total protein, albumin, globulin, total bilirubin); cholesterol, high density lipoprotein, low density lipoprotein, triglycerides, glucose and creatine kinase.

Body composition analysis

Evaluation of lean and fat mass was performed by using a 15.2 T MRI horizontal bore scanner and BFG6S-100 actively shielded gradient system (1 T/m maximum gradient strength (Bruker BioSpin MRI GmbH, Ettlingen, Germany). A 35 mm quadrature birdcage coil was used for both transmission and reception. All animals (SD: 6 months old; HFD: 5 months old and 1 month on HFD) were anesthetized with isoflurane (4% induction and 1.5% maintenance). Imaging was done using multi-slice spin echo sequence (TR/TE 800/4.01 ms, NAX = 2, 0.137 X 0.137 mm^2, 0.5 mm slice thickness, 2 averages). During imaging, respiration was monitored using small animal monitoring system (SA Instruments Inc., Stony Brook, NY), and the body temperature was maintained using circulating

water bath (Thermo Scientific). The lean and fat volume was calculated based on semi-automated segmentation of 2D images multiplied by slice thickness using AMIRA (V 6.0, Thermo Fisher Scientific).

Adipocyte size

Adipocyte size analyses was performed using H&E stained paraffin sections of epididymal and subcutaneous WAT pads (SD: 18 weeks old; HFD: 6 months old and 16 weeks on HFD). 50 adipocytes per fat pad section and four sections per mouse were analyzed by semi-automated morphometry (AxioVision morphometry software, Zeiss).

Food intake and feeding efficiency

Prior to recording of food intake, mice were single housed and let to acclimatize to new housing conditions for 2 weeks. Food intake and body weight gain of standard chow (2-5 months old) and high fat diet (3-9 months old and 1-16 weeks on HFD) fed animals were measured over several weeks. Feeding efficiency (1st month on HFD) was calculated as mg body weight gain per kcal food consumed. Data was excluded if food was spilled in the cage.

Absorption of dietary fat

To study intestinal absorption of dietary fat, mice (3-4 months old) were challenged with a bolus of 100 μL of olive oil containing 2 μCi 3H-triolein (Perkin Elmer) through intragastric gavage. To inhibit the clearance of plasma triacylglycerol, we administered i.p. 100 μL of the surfactant tyloxapol (5% in PBS, Sigma-Aldrich) 15 min before intragastric gavage. Blood was collected before (time 0) and at 1 h, 2 h and 4 h after intragastric gavage for scintillation counting (Ultima Gold solution measured using the Tri-Carb 4910TR liquid scintillation counter; Perkin Elmer).

Triglyceride (TG), non-esterified fatty acids (NEFA), corticosterone, thyroid-stimulating hormone (TSH), oxytocin and adiponectin measurements

The following kits were used to measure plasma TG, NEFA, corticosterone, TSH, oxytocin and adiponectin levels (SD: 4 months old; HFD: 6 months old and 16 weeks on HFD): Dialab triglycerides, GPO-PAP (D00390); WAKO (HR Series NEFA-HR(2)); Enzo Life Sciences corticosterone ELISA kit (ADI-900-097); EIAAB mouse thyrotropin subunit beta ELISA (E0463m); Enzo Life Sciences oxytocin ELISA kit (ADI-900-153A) and Quantikine mouse adiponectin/Acrp30 Immunoassay (MRP300).

Tissue triglyceride measurements. Tissue lipid extraction was performed using a slightly modified Folch method (Folch et al., 1957). In brief, approximately 50mg (±10mg) of snap frozen tissues (mice were 5 months old and 1 month on HFD) were homogenized using the "Precellys Evolution" bead homogenizer in 250μl ice-cold PBS, and subsequently mixed by vortexing with 750μl of a chloroform/methanol (2:1) solution, followed by a centrifugation step (21,000 g for 10 min at 4°C). The organic phase of the samples was transferred to a fresh glass tube. The organic solvents were vaporized under a nitrogen flow, and the resulting pellet resuspended in 250μl of chloroform (2% Triton-X v/v). After an additional vaporizing step at 50°C, we resolubilized the pellets in 100μl aqua bidest. TG abundance was measured using the widely employed GOP/PAP method, where glycerol is enzymatically cleaved from the acyl side chains and in further enzymatic reactions, a colorimetric shift is produced, corresponding to the concentration of the TG content (Roche Diagnostics).

Tissue NEFA measurements. For tissue extraction of non-esterified fatty acids (NEFAs), we used the recommended protocol of the Abcam free fatty acid kit (ab65341) (Becares et al., 2019; Scopelliti et al., 2019). A chloroform solution containing 1%Triton-X (v/v) was employed for lysing snap frozen tissue samples (mice were 5 months old and 1 month on HFD). The average weight of the utilized tissue was 20mg (±5mg). After cutting and weighing, the samples were lysed using the "Precellys Evolution" homogenizer until the lysate was homogeneous. Samples were incubated on ice for 10 min, centrifuged for 10 min at 21,000 g at 4°C, and consequently the organic phase was transferred to a fresh glass tube. We removed the organic phase by air-drying at 50°C in a fume hood. The pellet was resolubilized in the Abcam assay buffer and quantified using the Abcam free fatty acid kit.

Oral glucose tolerance test

Mice (SD: 3-4 months old; HFD: 5 months old and 3 months on HFD) were fasted overnight and administered an oral glucose bolus by gavage (2g/kg for standard chow fed mice and 1g/kg for high fat diet fed mice). Blood glucose concentrations were measured every 15 min over a time range of one h using a handheld blood glucose meter (One Touch UltraEasy; Lifescan). For analysis of insulin levels, tail vein blood samples were added to a NaCl/EDTA solution to avoid blood clotting and plasma insulin concentrations were determined using the Alpco Mouse Ultrasensitive Insulin ELISA (80-INSMSU-E10).

Thermoneutrality

At the age of 8 weeks, male *Alk*$^{+/+}$ and *Alk*$^{-/-}$ mice were single housed in SMI type2 long standard filtertop cages and transferred to a climate chamber (Memmert, HPP 750) set to 30°C and 12/12 h light/dark cycle. Animals were fed *ad libitum*, checked daily by veterinary staff and body weight was recorded once a week.

Analysis of sterols in feces

Fecal samples collected from individually housed mice over a 24 h (SD fed mice; 4 months old) or 48 h (HFD fed mice; 5 months old and 3 months on HFD) period were dried, weighed and thoroughly grounded. An internal standard (49 nmol of 5α-cholestane) was added to 50mg of feces followed by the addition of 250μl 1M sodium hydroxide and 750μl methanol. Samples were heated to 80°C and then extracted 3 times with petroleum ether 60-80, each time collecting the ether fractions, which were subsequently evaporated under a stream of nitrogen. After adding a mixture of BSTFA, pyridine and TMCS (5:5:0.1) followed by evaporation again under a stream of nitrogen, heptane was added to the samples and they were analyzed for neutral sterols by gas liquid chromatography (Agilent, Santa Clara, CA, USA). The water layer from the extraction was transferred to Sep-Pak C18 cartridges, flushed out with 75% methanol and then the eluate was evaporated under a stream of nitrogen. 200μl of methanol and acetyl chloride (1:20) were added

to the tubes, the mixture was heated to 55°C and then dried again under a stream of nitrogen. Derivatization was performed exactly as for neutral sterols and samples were analyzed by gas liquid chromatography.

Indirect calorimetry

All measurements were performed at room temperature (21°C-23°C) on a 12/12 h light/dark cycle in a PhenoMaster System (TSE systems, Bad Homburg, Germany) using an open circuit calorimetry system and animals were checked daily by veterinary staff. Mice (4-7 months old; 2-14 weeks on HFD) were housed individually, trained on drinking nozzles for 72 h and allowed to adapt to the PhenoMaster chamber for 2 days. Food and water were provided *ad libitum* in the appropriate devices and measured by the build-in automated instruments. Parameters of indirect calorimetry and activity were measured for 5 consecutive days. Body weight was recorded at the beginning and end of the experiment and averaged values were blotted against energy expenditure and activity data as guidelines for experimental design for indirect calorimetry recommended (Tschöp et al., 2011).

Mouse tissue library

An in-house made mouse tissue library (n = 3 mice) was used to analyze the tissue distribution of mouse *Alk* mRNA expression. Mouse total RNA was prepared from 8 weeks old B6J mice purchased from Jackson Laboratory and reverse transcribed to cDNA. Post-amplification melting curve analysis was performed to check for unspecific products. For normalization, *Alk* threshold cycles (Ct-values) were normalized to *Rplp0* (ribosomal protein, large P0;) within each sample to obtain sample-specific ΔCt values (= Ct *gene of interest* – Ct *housekeeping gene*). $2^{-\Delta\Delta Ct}$ values were calculated to obtain fold expression levels.

Hypothalamic serial sections and LacZ staining

Mice (SD; 4 months old) were euthanized with CO2 and perfused with 2% paraformaldehyde (PFA). Dissected brain tissue was fixed overnight at 4°C in 2% PFA and embedded in 1.5% low melting agarose (in PBS). The hypothalamic area was cut into 50μM sections using a vibratome. Sections were stored in PBS. Upon removal of PBS, sections were incubated overnight in LacZ staining solution at 37°C. A paint brush was used to transfer sections into a dish containing PBS (= washing) and then onto slides. Sections on slide were dried at room temperature and post-fixed in 4% PFA. Sections were then counterstained using Nuclear Fast Red, washed in H2O and stepwise dehydrated in 30, 70, 80, 95 and 100% EtOH followed by an incubation in xylene for one minute each. The following LacZ staining solution was used: 44mL PBS; 2mL K3 (potassium ferricyanide; 500mM); 2mL K4 (potassium ferrocyanide; 500mM); 0,5mL Na-deoxycholate (1%); 0,1mL MgCl (1M); 10 μL NP-40; 1,25mL Bluo-Gal (100mg in 2,5mL dimethylformamide).

Norepinephrine (NE) measurements

Quantification of mouse (7-11 months old) adipose tissue norepinephrine levels was performed by hydrophilic interaction liquid chromatography (HILIC-QTOF) mass spectrometry by the West Coast Metabolomics Center (UC Davis) and human adipose samples were analyzed by the NeuroChemistry Core at Vanderbilt University.

Single-cell RNA-seq data generation and analysis

Data were generated on C57Bl6/N mice of both sexes on postnatal days 10-23. Single-cell RNA-seq by the 10x Genomics Chromium Single Cell Kit (version 2) was performed on methanol-fixed cells that had been dissociated with the Papain Dissociation System (Worthington). High-throughput RNA sequencing was performed on an Illumina HiSeq3000 instrument. We used published criteria on hypothalamic neuronal heterogeneity (Simmons and Swanson, 2009) to distinguish major magnocellular and parvocellular neuronal subtypes of the paraventricular nucleus of the hypothalamus by using positional marks of the PVN (such as, e.g., the lack of clock genes and c-*fos* expression otherwise characterizing Oxt+ and Avp+ neurons of the suprachiasmatic and supraoptic nuclei and lack of Onecut3 transcription factor for Sst neurons (Romanov et al., 2017)): five cell groups (Figure 5C) were obtained and processed by the *SCT-pipeline* of *Seurat 3.1* package (Hafemeister and Satija, 2019; Stuart et al., 2019) and visualized by uniform manifold approximation and projection (UMAP) algorithm (McInnes et al., 2018). A log-normalized expression matrix was used to derive differentially expressed genes (DEGs) for each neuronal group against a background with Student's t test using Bonferroni correction for all genes in the dataset (Table S5). Expression of genes associated with inhibitory GABAergic neurons (*Gad1*) and excitatory glutamatergic neurons (*Slc17a6*) were correlated with *Alk* expression. The composition of *Alk* positive cells was determined by inspecting the occurrence of marker genes characteristic for PVN cell populations as intersection sets (Conway et al., 2017). Finally, major neuropeptide/hormone, neuropeptide receptor and *Alk* signaling determinants in each of the five major PVN clusters (*Oxt, Avp, Crh, Trh, Sst*) were defined.

Enhancer (luciferase reporter) assay

$5x10^5$ SH-SY5Y cells (Sigma #94030304) were electroporated via Maxcyte STX (Cat No. GOC1) with the "luciferase reporter vector" (Addgene ID #99297) utilizing the ORI as a core promoter (Muerdter et al., 2018) comprising either the putative identified enhancer region spanning the *ALK* indel rs568057364 or a negative control (Addgene ID #99315) together with a Renilla control vector (Promega # E2261) in a ratio of 10 to 1. After 25min recovery time at 37°C, cells received medium (dmem/f12 supplemented with l-glutamine and 10% fcs) and 1x105 cells were diluted into 6well plates. 6h later cells were collected, centrifuged at 500 g and washed with 1xPBS. PBS was removed and cells were lysed using QIAshredder columns (QIAGEN #79654) followed by total RNA extraction via the RNeasy mini prep kit (QIAGEN #74104), with beta-Mercaptoethanol supplemented RLT buffer. 1.5μg of isolated total RNA was treated with TurboDNase (Invitrogen Cat No. AM2238) for 30min at 37°C in a thermocycler. Afterward, 2μl DNase inactivation reagent (Ambion #AM1906) was added and vortexed for 2min, with 20sec breaks within, and centrifuged for 5min at 10,000 g. 10μl of RNA were added to the reverse transcription reaction mixture containing 1μl dt18 (NEB #S1316S), 1μl dNTPs (NEB #4475), 1μl RNase Inhibitor (Thermo Fisher #EN0531), 1μl SuperScript III (Invitrogen #18080093), 1μl DTT (Invitrogen #18080093; within SSIII kit), 4μl forward strand buffer (Invitrogen #18080093, within SSIII kit) and 1μl H_20. Reaction was mixed and heated to

25°C for 5min, 50°C for 50min, 70°C for 15min and 4°C for 10min in a thermocycler. Afterward samples got diluted to a total of 100µl and 2µl were used for qPCR. Reaction setup/sample: 10µl SybrGreen (Thermo Fisher #4309155), 1µl forward (10µM), 1µl reverse primer (10µM), 7µl H_20 and 2µl cDNA. qPCR setup/whole plate: 95°C 2sec, 95°C 3min, 60°C 30sec, read plate, go back to step 2 for 39 times (40 cycles in total). Post-amplification melting curve analysis was performed to check for unspecific products. For normalization, *Firefly* threshold cycles (Ct) values were normalized to *Renilla* Ct values and the normalized negative control values were set as 1 and the DNA fragment spanning *ALK* variant rs568057364 values were presented as fold change.

Stereotaxic surgery for intracerebral viral vectors delivery

Alk$^{fl/fl}$ male mice (2-3 months old) were anaesthetized with isoflurane (5%, Abbot Laboratories) and fixed in a stereotaxic frame (Kopf). Anesthesia throughout the procedure was delivered via mouth tubing and maintained between 1.6 and 2.2% of isoflurane in the air. The body temperature was monitored with a rectal thermometer and kept constant at 36°C by a heating pad (DC temperature controller). The mouse head was shaved and 0.1ml of the local anesthetic Xylanaest 0.5% (Gebro Pharma) injected subcutaneously. The skull was exposed, cleaned and small holes were drilled bilaterally above the PVN, at coordinates: AP −0.82, ML ± 0.35, DV −4.9, relative to bregma (Paxinos and Franklin, 2007). Mice were injected with 45nl/injection site of 1:10 mixture of AAV::DIO-GFP (Cre-dependent GFP, 0.1 × 10^{11} GC/mL) and AAV::Cre (1 × 10^{12} GC/mL) viral vectors; control mice received injection of AAV::GFP (1.15 × 10^{13} GC/mL). Vectors were delivered to the PVN via a thin glass pipette and the injection was controlled by a Micro4 Micro Syringe Pump (World Precision Instruments; injection volume 45nl/site, delivery rate 15nl/min). To prevent backflow, the pipette was left at the injection site for 3 min after the injection was finished. Mice were let to recover for at least one week after the surgery and during that time their drinking water was supplied with enrofloxacine 0.1mg/mL (Baytril, Bayer) and caprofen 0.2mg/mL (Rimadyl, Pfizer). At the end of the experiment, mice were euthanized using CO_2 followed by histological validation of correct viral targeting of the PVN.

Western blotting

Fasted mice were sacrificed by cervical dislocation and tissues were snap frozen in liquid nitrogen. Figures 6D and 6I and S8H: SD; 4 months old. Figure 6E: 5 months old and 8 weeks on HFD. Figure 6H: 6 months old and 14 weeks on HFD. Mouse tissues were homogenized in RIPA buffer (Sigma; R0278) containing Halt protease and phosphatase inhibitor cocktail (Thermo Scientific; 78440). Western blotting was carried out using standard protocols. Blots were blocked for 1 h with 5% Phosphoblocker Blocking Rgnt (Cell Biolabs; AKR-103) in TBST (1 × TBS and 0.1% Tween-20) and were then incubated overnight at 4°C with primary antibodies diluted in 5% Phosphoblocker in TBST (1:1000 dilution). Blots were washed three times in TBST for 15 min, then incubated with HRP-conjugated secondary antibodies diluted in 5% Phosphoblocker in TBST (1:2500 dilution) for 45 min at room temperature, washed three times in TBST for 15 min and visualized using enhanced chemiluminescence (ECL Plus, Pierce, 1896327). The following primary antibodies were used: monoclonal anti-β-actin (Sigma, A5316); anti-HSL (Cell Signaling, 4107), anti-phospho-HSL (Ser660) (Cell Signaling, 4126) and anti-Ucp1 (Abcam, ab10983). Secondary antibodies were anti-rabbit IgG HRP (GE Healthcare, NA9340V) and anti-mouse IgG HRP (Promega, W4021). Quantification of western blot bands was performed by selection of equal sized areas of Ucp1 and Actin. The positively stained area was quantified using the gel analysis tool in ImageJ and the ratio of Ucp1 and Actin was calculated.

Quantitative PCR

Figure 5B: Mouse tissues (SD: 4 months old) were snap frozen in liquid nitrogen. RNA was extracted using RNeasy Mini Kit from QIAGEN and reverse-transcribed into cDNA using the iScript cDNA synthesis kit from BioRad. qPCR reactions were performed in the CFX384 Real-Time PCR Detection System (BioRad) using the GoTaq qPCR Master Mix (Promega). Post-amplification melting curve analysis was performed to check for unspecific products. For normalization, threshold cycles (Ct-values) were normalized to *Hprt* within each sample to obtain sample-specific ΔCt values (= Ct *gene of interest* – Ct *housekeeping gene*). $2^{-\Delta\Delta Ct}$ values were calculated to obtain fold expression levels. Fasted values were set as 100% and refed values were presented as percentage change.

Figures 6F and 6G and S8I: Mouse tissues (SD: 4 months old; HFD: 4 months old and 1 month on HFD) were snap frozen in liquid nitrogen. Total RNA was extracted from tissue using TRIzol (Thermo Scientific #15596018) and treated with DNase I (Thermo Scientific #EN0521) for genomic DNA digestion prior cDNA synthesis. 1µg of total RNA was reverse transcribed to cDNA using a cDNA synthesis kit (RevertAid RT Kit, Thermo Scientific #K1691) according to the manufacturer's protocol. Gene expression was analyzed by quantitative real-time RT-PCR (FastStart Universal SYBR Green Master (ROX), Roche #04913914001) using a QuantStudio 6 RealTime PCR System (Applied Biosystems). Post-amplification melting curve analysis was performed to check for unspecific products. For normalization, threshold cycles (Ct-values) were normalized to *36B4* within each sample to obtain sample-specific ΔCt values (= Ct *gene of interest* – Ct *housekeeping gene*). $2^{-\Delta\Delta Ct}$ values were calculated to obtain fold expression levels. Wild-type values were set as 1 and knockout values were presented as fold change.

Figure S8K: Mouse tissues (5 months old; 1 month on HFD) were snap frozen in liquid nitrogen. Total RNA was extracted using PeqGold Trifast (VWR) and reverse transcribed with M-MLV Reverse Transcriptase (Thermo Fisher Scientific) according to the manufacturer's protocols. Real-time PCR reactions were performed using a universal probes mix (BioRad) on a CFX cycler and analyzed with CFX software (BioRad). For normalization, threshold cycles (Ct-values) were normalized to *Rpl4*, *Oaz1* and *Rpl13a* within each sample to obtain sample-specific ΔCt values (= Ct *gene of interest* – Ct *housekeeping gene*). $2^{-\Delta\Delta Ct}$ values were calculated to obtain fold expression levels. Wild-type values were set as 1 and knockout values were presented as fold change.

QUANTIFICATION AND STATISTICAL ANALYSIS

Calculation of IBS relationships between samples and identification of relatedness

Estimate of IBS (identity by state) between each pair of samples, based on a pruned subset of SNPs, was required to evaluate the extent of relatedness between samples. This pruned subset of SNPs was obtained by following the steps below:

Prune extracted SNPs for r2 > 0.2 using a sliding window of 50 SNPs with a 5 SNP overlap (PLINK command options–indep 50 5 1.25). Estimation of IBS was achieved by using plink: plink–bfile mydata.pruned–Z-genome. We can then identify all pairs of samples with pi_hat > 0.3 as "related" (threshold may vary between cohorts). For each pair of samples with pi_hat > 0.3, samples were selected for exclusion using the following criteria: 1) Exclude any sample that is related to more than one other sample; 2) Exclude the sample with lowest call rate on the basis of all variants passing QC.

Calculation of principal components

Principal components (PCs) were calculated to identify ethnic outliers and to evaluate the extent of population stratification within cohorts. Principal components were constructed on the basis of the IBS estimated in the previous step using the pruned subset of SNPs. The PLINK v1.9 command line was: "plink -bfile egcut_data -read-genome egcut_data.pruned.genome.gz -cluster-mds-plot 10". The projection of each sample was recorded onto the first ten principal components (PCs) for use in downstream analyses to adjust for population structure. Clear non-European outliers were excluded. For scatterplot, 1000 Genomes CEU, YRI and CHB/JPT were used for anchoring.

Genome-wide association analyses

Statistical analysis was performed with SNPTEST (Marchini et al., 2007), using the method 'expected'. Covariates included gender, age and the four first components from a Principal Component Analysis on genotype data (to account for possible population stratification).

Two case-control analyses (logistic regression) were performed:

ANALYSIS 1: healthy thin as cases and healthy control weight subjects (controls) as controls**;** healthy thin ~SNP + sex + age + population stratification PCs.

ANALYSIS 2: healthy overweight and/or obese subjects as cases and healthy normal weight subjects (controls) as controls; healthy overweight and/or obese ~SNP + sex + age + population stratification PCs.

Upon analysis, no abnormal p value inflations were seen on QQ plots (not shown).

Further analyses of the *ALK* indels

Conditional analyses

These analyses were performed to evaluate whether the ALK indels would remain associated with the thinness status (relative to healthy controls) when adjusting for 4 ALK variants associated with BMI. Analyses were performed using the following logistic regression; controls**;** healthy thin ~SNP + age + sex + population stratification PCs + 4 ALK variants associated with BMI.

Interaction with age

These analyses aimed to evaluate whether the ALK genetic effect from our indels, was dependent on the subject's age. Analyses were performed using the following logistic regression; controls**;** healthy thin ~SNP * age + sex + population stratification PCs.

UKBB data analysis

UK Biobank data was analyzed as a part of project 17085. Non-European ancestry was used as exclusion criteria. The age distribution in the UKBB was significantly higher than in the EGCUT biobank (age range of 40-69 with the youngest individual being 37 years old). To align the data with our current analysis we only considered the age group 41-45 which showed a similar BMI distribution as the respective age group in the Estonian biobank. Sample size of the thin individuals by selecting the 6th lowest percentile was 2527 individuals (1167 male and 1360 females) and 8430 (3898 males and 4532 females) for the control individuals (30-50th percentile). The analysis was performed using BOLT-LMM v2.3 software using sex, age and the first 15 PCs as covariates (Loh et al., 2018).

Functional analyses of variants

Brain Almanac Analyses

Expression in 10 different brain regions and genotype were retrieved for 134 subjects from the Brain Almanac (http://www.braineac.org/) (Huckins et al., 2019). Missing expression values were imputed using chained-equation (using MICE (van Buuren and Groothuis-Oudshoorn, 2011), with settings m = 5, maxit = 50, method = pmm). Subsequent eQTL analyses focused on the t2546409 probeset and used the MatrixEQTL (Shabalin, 2012) package with a linear model. Next, for SNPs displaying at least R-square > 50% with our indels, we performed a multi-marker analysis using GATES (Li et al., 2011), as implemented in the aSPU R package (Pan et al., 2014).

ALK variant annotations

Molecular QTL (p-/e-/m-QTL) and overlap with published GWA hits for the *ALK* variants were retrieved from the PhenoScanner (Kamat et al., 2019; Staley et al., 2016) database. Allele frequencies and LD relationship for our two indels in different populations were retrieved from the 1000G project (Auton et al., 2015) using the LDlink portal (https://ldlink.nci.nih.gov/) (Machiela and Chanock, 2015).

Epigenomic state prediction

Chromatin state annotation of the locus around the two top *ALK* indels was evaluated using the Epigenome browser (https://epigenomegateway.wustl.edu/; (Li et al., 2019)). PrimaryHMM tracks (15 state core model) from the public data hub were used to visualize the regulatory state of the different human cell lines and tissues form the Roadmap Epigenomic Project.

Statistical analysis of mouse studies

All mouse data are expressed as mean ± standard error of the mean (SEM). Statistical significance was tested by Student's two tailed, unpaired t test; Mann-Whitney U test; 2-way ANOVA followed by Bonferroni's post hoc test or Analysis of Co-Variance (ANCOVA) using body weight as covariate where appropriate (Tschöp et al., 2011). All figures and mouse statistical analyses were generated using Prism 8 (GraphPad) or R. Details of the statistical tests used are stated in the figure legends. In all figures, statistical significance is represented as $^{*}p < 0.05$, $^{**}p < 0.01$, $^{***}p < 0.001$, $^{****}p < 0.0001$.

Supplemental Figures

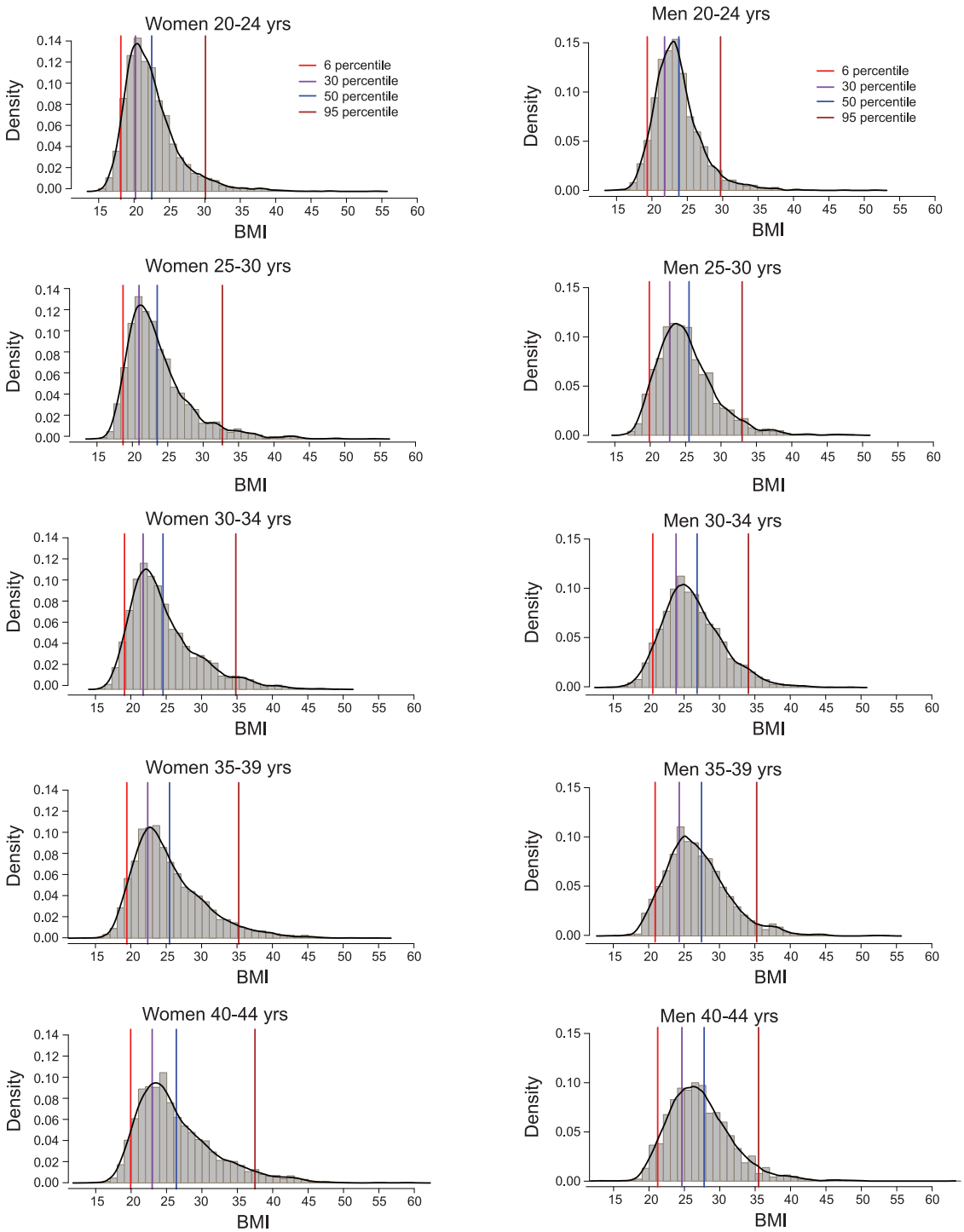

Figure S1. BMI Histograms by Strata of Five Years (from 20 to 44 years) in the EGCUT Biobank Database Grouped by Gender, Related to Figure 1

The different percentiles of BMI distribution at the indicated age groups are shown. The Y axes indicate population densities of the different BMI distributions at the assorted age strata. Colored vertical lines show the respective limit cut offs for each category.

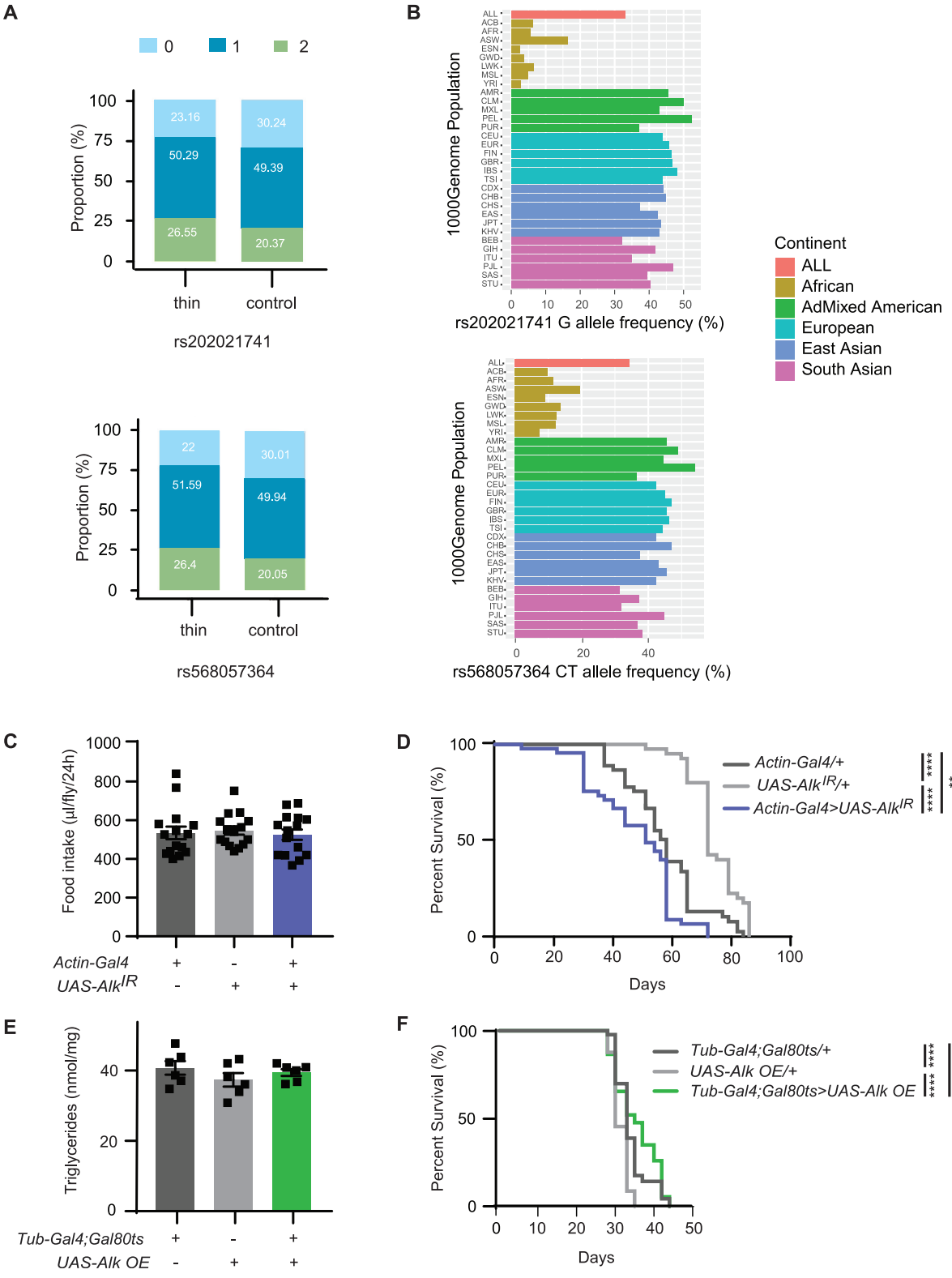

Figure S2. Genotype Proportions, Allele Frequencies, and Basic Fly Studies, Related to Table 1, Table S1, and Figure 2

(A) rs202021741 and rs568057364 proportions in the thin and control group in the EGCUT cohort. 0 (light blue) corresponds to the homozygous non-effect allele, 1 (dark blue) to the heterozygous and 2 (green) to the homozygous effect allele. (B) Allele frequencies in different worldwide populations (obtained from the 1000

(legend continued on next page)

Genomes projects) of the two top *ALK* variants. Analysis of food intake (C, n = 15 replicates) and lifespan (D, n = 45 flies) of *Alk* RNAi knockdown flies. Over-expression of *Alk* in flies has no apparent effect on triglyceride levels and lifespan (E, n = 6 replicates and F, n = 90 flies). Data are presented as mean ± SEM.; $^{**}p < 0.01$, $^{****}p < 0.0001$; One-way ANOVA with Bonferroni's multiple comparisons test (C and E) and Log-rank (Mantel-Cox) test (D and F).

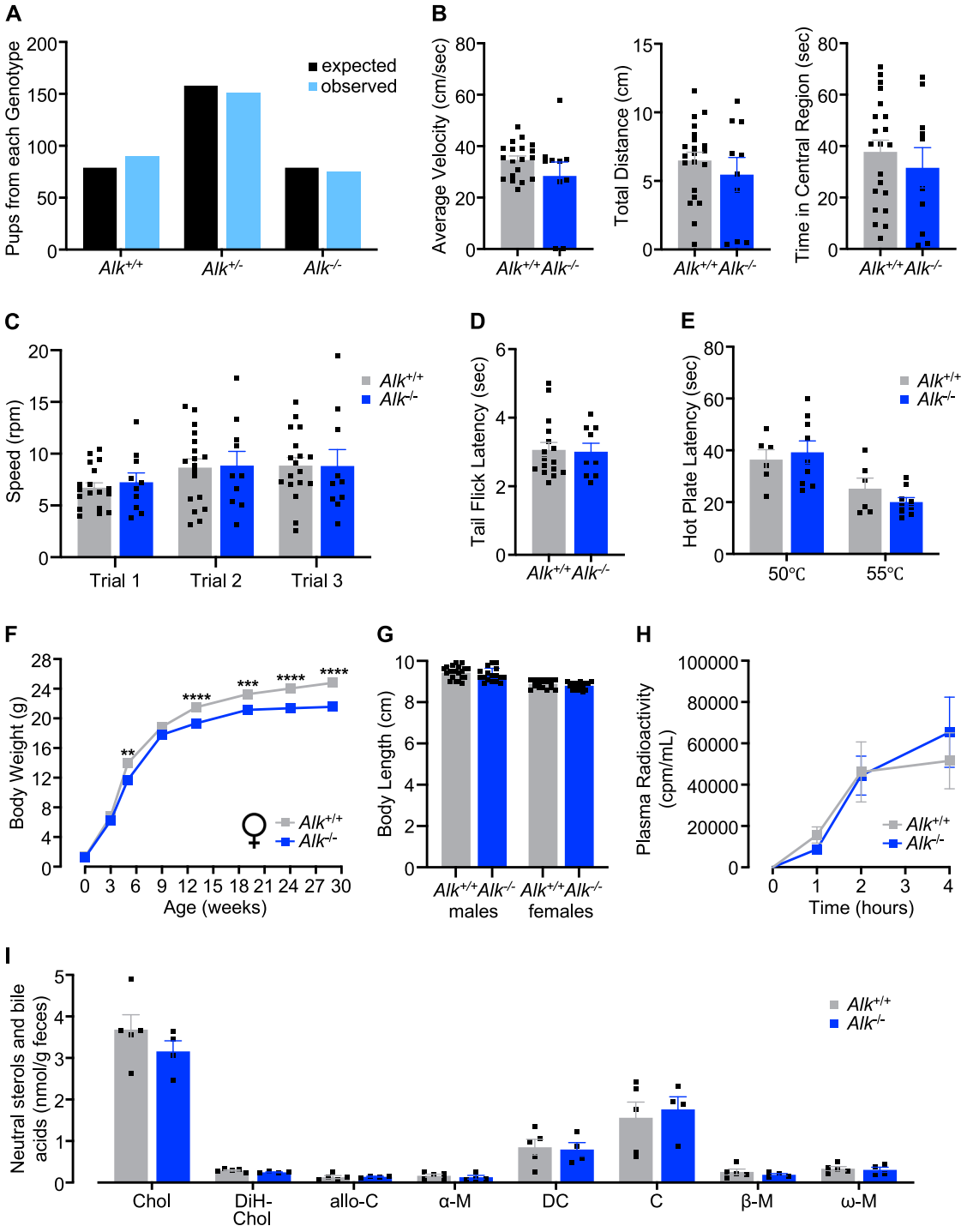

Figure S3. Phenotypic and Behavioral Characterization of *Alk*$^{-/-}$ Mice, Related to Figure 3

(A) The number of mice of various genotypes obtained by the Alk$^{+/-}$ intercross is shown. (B-E) *Alk*$^{+/+}$ and *Alk*$^{-/-}$ mice were evaluated for phenotypic changes by testing on multiple behavioral tasks: Open field test (B), Rotarod test (C), Tail flick test (D) and Hot plate test (E) ($n \geq 6$; 10-12 weeks old). Speed in (C) describes the velocity at which mice fell of the rotarod. (F) Body weight curves of female *Alk*$^{+/+}$ and *Alk*$^{-/-}$ mice on SD ($n \geq 7$). (G) Body length of 2 months old male and female *Alk*$^{+/+}$ and *Alk*$^{-/-}$ mice on SD ($n \geq 15$). (H) Assessment of intestinal triglyceride uptake. Tyloxapol-treated mice were challenged with an oral olive oil bolus containing 2 μCi 3H-triolein and plasma radioactivity was recorded over a 4 h time period ($n \geq 12$). (I) Quantification of neutral sterols and bile acid content in the feces by gas liquid chromatography ($n \geq 4$). Chol, cholesterol; DiH-Chol, dihydrocholesterol; allo-C, allocholic acid; α-M, alpha-muricholic acid; DC, deoxycholic acid; C, cholic acid; β-M, beta-muricholic acid; ω-M, omega-muricholic acid. All data are presented as mean ± SEM.; $^{**}p < 0.01$, $^{***}p < 0.001$, $^{****}p < 0.0001$; Student's two tailed, unpaired t test (B-E and G); 2way ANOVA followed by Bonferroni's multiple comparisons test (F, H and I).

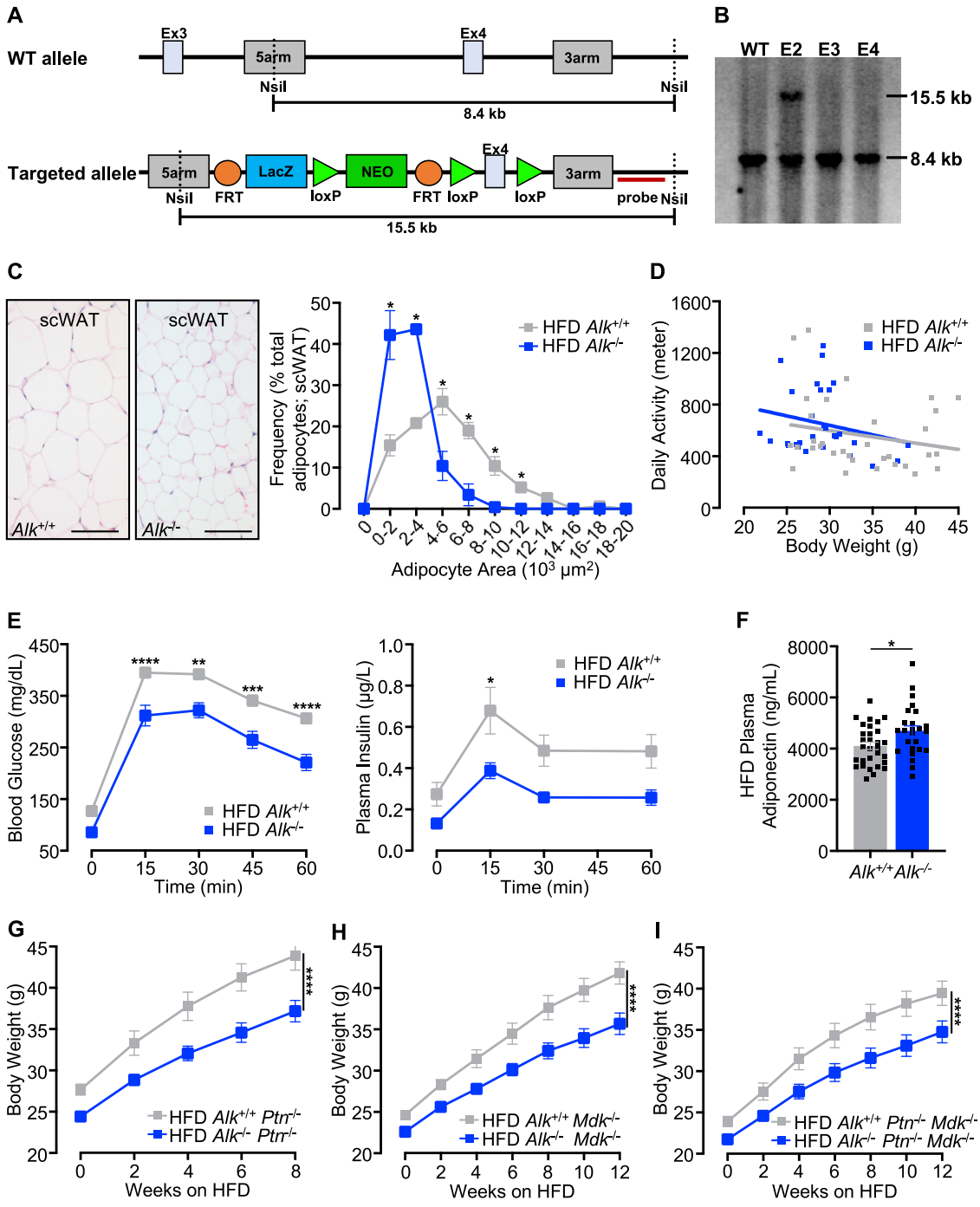

Figure S4. Metabolic Parameters of *Alk* Knockout Mice, Related to Figure 4

(A) Gene targeting strategy for the generation of the conditional *Alk* mutant allele. (B) Southern blot of genomic ES cell DNA reveals clone E2 to be correctly targeted. Clone E2 was injected into blastocysts to generate Alk^{flox} mice. (C) Representative pictures of hematoxylin and eosin stained adipose tissue sections (left panels) and analysis of adipocyte cell size (right panels) of scWAT (n = 5; 16 weeks on HFD). Scale bar = 100µm. (D) Analysis of daily activity using indirect calorimetry ($n \geq 28$). (E) Blood glucose (left panel; $n \geq 12$) and plasma insulin (right panel; $n \geq 7$) levels of HFD fed mice following an oral glucose bolus. (F) Quantification of plasma adiponectin levels in HFD fed mice ($n \geq 25$). (G) Body weight curve of *Pleiotrophin* single ($Alk^{+/+}$ $Ptn^{-/-}$) and *Alk* plus *Pleiotrophin* double mutant ($Alk^{-/-}$ $Ptn^{-/-}$) mice fed a HFD ($n \geq 9$). (H) Body weight curves of *Midkine* single mutant ($Alk^{+/+}$ $Mdk^{-/-}$) and *Alk* plus *Midkine* double mutant ($Alk^{-/-}$ $Mdk^{-/-}$) mice fed a HFD ($n \geq 9$). (I) Body weight curve of $Alk^{+/+}$ $Ptn^{-/-}$ $Mdk^{-/-}$ and $Alk^{-/-}$ $Ptn^{-/-}$ $Mdk^{-/-}$ triple mutant mice fed a HFD ($n \geq 9$). Data are presented as mean ± SEM.; $*p < 0.05$, $**p < 0.01$, $***p < 0.001$, $****p < 0.0001$; Student's two tailed, unpaired t test (F); Mann-Whitney U test (C), 2way ANOVA followed by Bonferroni's multiple comparisons test (E and G-I) and Analysis of Co-Variance (ANCOVA) using body weight as covariate (D).

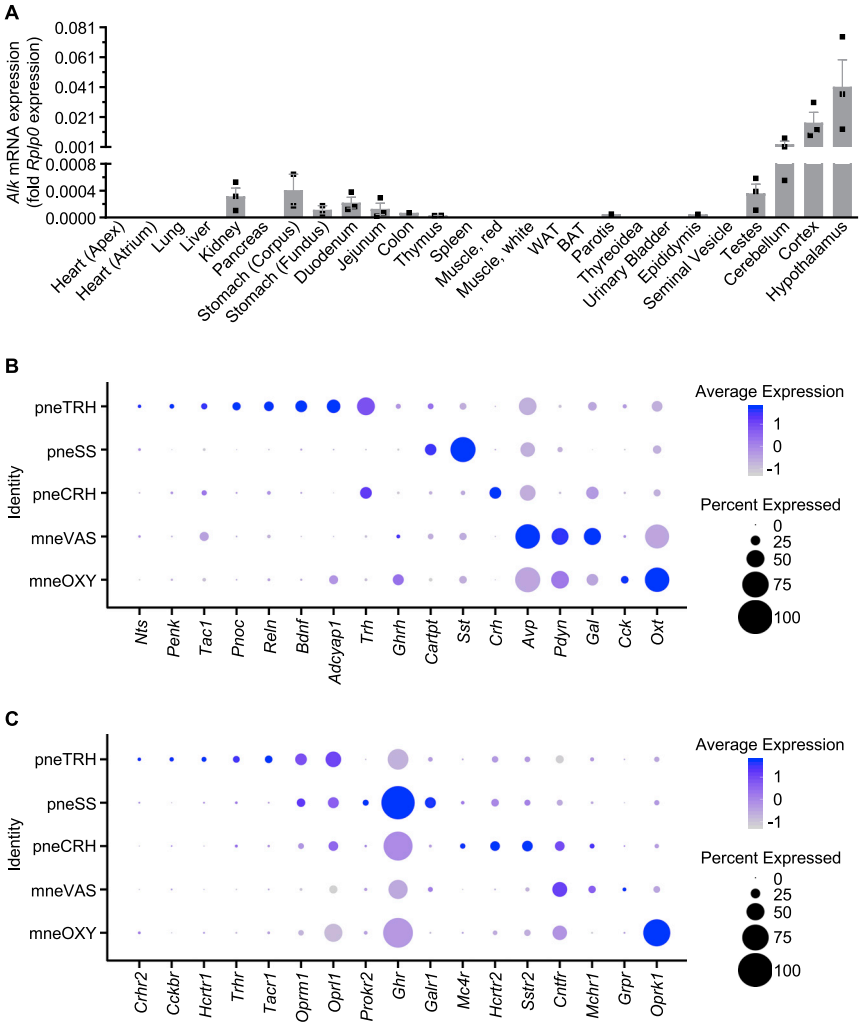

Figure S5. RT-qPCR Analysis of *Alk* mRNA Expression and Gene Expression Analysis of the Five Neuronal PVN Populations, Related to Figure 5

(A) *Alk* expression in the indicated tissues, showing low levels of *Alk* expression in kidney, stomach, duodenum, jejunum, colon, thymus, parotis, epididymis, testes, and higher levels of expression in the cerebellum, cortex and hypothalamus. Tissue *Alk* mRNA levels were normalized to *Rplp0* (ribosomal protein, large P0) mRNA levels and data are presented as fold *Rplp0* expression (n = 3 mice). Dot-plot representation of differential gene expression of neuropeptides (B) and neuropeptide receptors (C) in the 5 defined PVN populations. *Nts (neurotensin), Penk (preproenkephalin), Tac1 (tachykinin 1), Pnoc (prepronociceptin), Reln (reelin), Bdnf (brain derived neurotrophic factor), Adcyap1 (adenylate cyclase activating polypeptide 1), Trh (thyrotropin releasing hormone), Ghrh (growth hormone releasing hormone), Cartpt (CART prepropeptide), Sst (somatostatin), Crh (corticotropin releasing hormone), Avp (arginine vasopressin), Pdyn (prodynorphin), Gal (galanin and GMAP prepropeptide), Cck (cholecystokinin), Oxt (oxytocin), Crhr2 (corticotropin releasing hormone receptor 2), Cckbr (cholecystokinin B receptor), Hcrtr1 (hypocretin (orexin) receptor 1), Trhr (thyrotropin releasing hormone receptor), Tacr1 (tachykinin receptor 1), Oprm1 (opioid receptor, mu 1), Oprl1 (opioid receptor-like 1), Prokr2 (prokineticin receptor 2), Ghr (growth hormone receptor), Galr1 (galanin receptor 1), Mc4r (melanocortin 4 receptor), Hcrtr2 (hypocretin (orexin) receptor 2), Sstr2 (somatostatin receptor 2), Cntfr (ciliary neurotrophic factor receptor), Mchr1 (melanin-concentrating hormone receptor 1), Grpr (gastrin releasing peptide receptor) and Oprk1 (opioid receptor, kappa 1).* Expression values are scaled and presented as dot's color; proportions of cells expressing the gene are presented as dot's size. Data in (A) are presented as mean ± SEM.

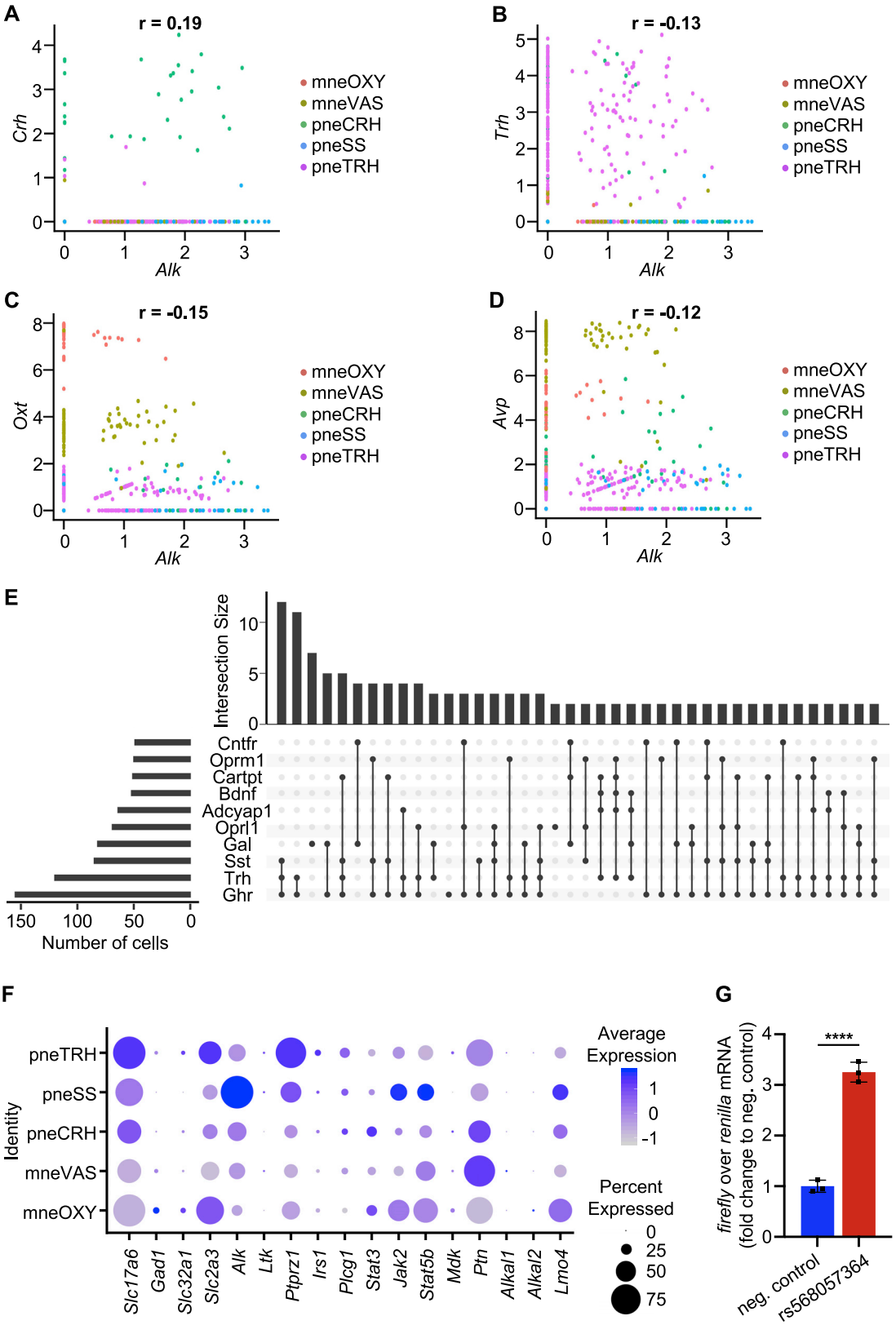

(legend on next page)

Figure S6. Gene Expression Analysis of *Alk*$^+$ Neurons, Related to Figure 5

Scatterplots showing coexpression of *Alk* and *Crh* (*corticotropin releasing hormone*; A), *Trh* (*thyrotropin releasing hormone*; B), *Oxt* (oxytocin; C) or *Avp* (*arginine vasopressin*; D) in the 5 defined neuronal populations of the PVN. (E) *Upset* plot showing gene expression analysis of *Alk*$^+$ neurons in the PVN (*Ghr, Trh, Sst, Gal, Oprl1, Adcyap1, Bdnf, Cartpt, Oprm1 and Cntfr*). (F) Assessment of differential gene expression of glutamatergic and GABAergic markers and known constituents of the ALK signaling pathway in the 5 neuronal populations of the PVN. *Slc17a6, Gad1, Slc32a1 (solute carrier family 32, member 1), Slc2a3 (solute carrier family 2, member 3), Alk, Ltk (leukocyte tyrosine kinase), Ptprz1 (protein tyrosine phosphatase, receptor type Z, polypeptide 1), Irs1 (insulin receptor substrate 1), Plcg1 (phospholipase C, gamma 1), Stat3 (signal transducer and activator of transcription 3), Jak2 (Janus kinase 2), Stat5b (signal transducer and activator of transcription 5b), Mdk, Ptn, Alkal1 (ALK and LTK ligand 1), Alkal2 (ALK and LTK ligand 2) and Lmo4 (LIM domain only 4).* Expression values are scaled and presented as dot's color; proportions of cells expressing the gene are presented as dot's size. Pearson's r correlation coefficient (A-D). (G) Enhancer activity of a DNA fragment spanning *ALK* indel rs568057364. mRNA levels of *firefly* were normalized to *renilla* (transfection control) expression and data are presented as fold change. Data are presented as mean ± SEM.; ****$p < 0.0001$; Student's two tailed, unpaired t test (G).

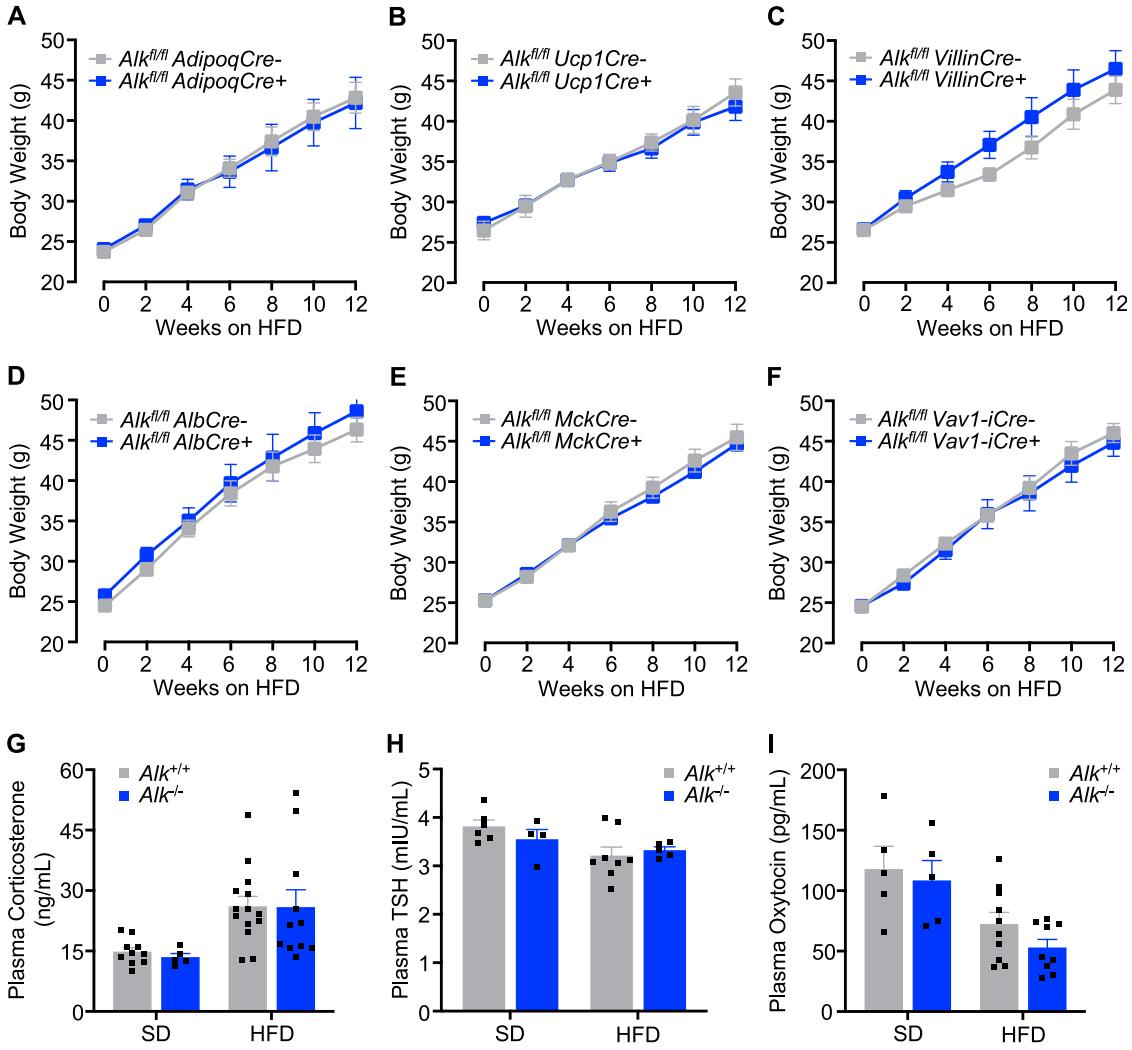

Figure S7. Body Weight Curves of Tissue-Specific *Alk* Knockout Mice, Related to Figure 5

(A) Body weight curves of *Alk*$^{fl/fl}$*AdipoqCre-* and *Alk*$^{fl/fl}$*AdipoqCre+* mice fed a HFD (n ≥ 6). (B) Body weight curves of *Alk*$^{fl/fl}$*Ucp1Cre-* and *Alk*$^{fl/fl}$*Ucp1Cre+* mice fed a HFD (n ≥ 5). (C) Body weight curves of *Alk*$^{fl/fl}$*VillinCre-* and *Alk*$^{fl/fl}$*VillinCre+* mice fed a HFD (n ≥ 8). (D) Body weight curves of *Alk*$^{fl/fl}$*AlbCre-* and *Alk*$^{fl/fl}$*AlbCre+* mice fed a HFD (n ≥ 6). (E) Body weight curves of *Alk*$^{fl/fl}$*MckCre-* and *Alk*$^{fl/fl}$*MckCre+* mice fed a HFD (n ≥ 7). (F) Body weight curves of *Alk*$^{fl/fl}$*Vav1-iCre-* and *Alk*$^{fl/fl}$*Vav1-iCre+* mice fed a HFD (n ≥ 7). Quantification of plasma corticosterone (G), TSH (H) and oxytocin (I) levels of SD and HFD fed mice (n ≥ 5). Data are presented as mean ± SEM.; Student's two tailed, unpaired t test (G-I); 2way ANOVA followed by Bonferroni's multiple comparisons test (A-F).

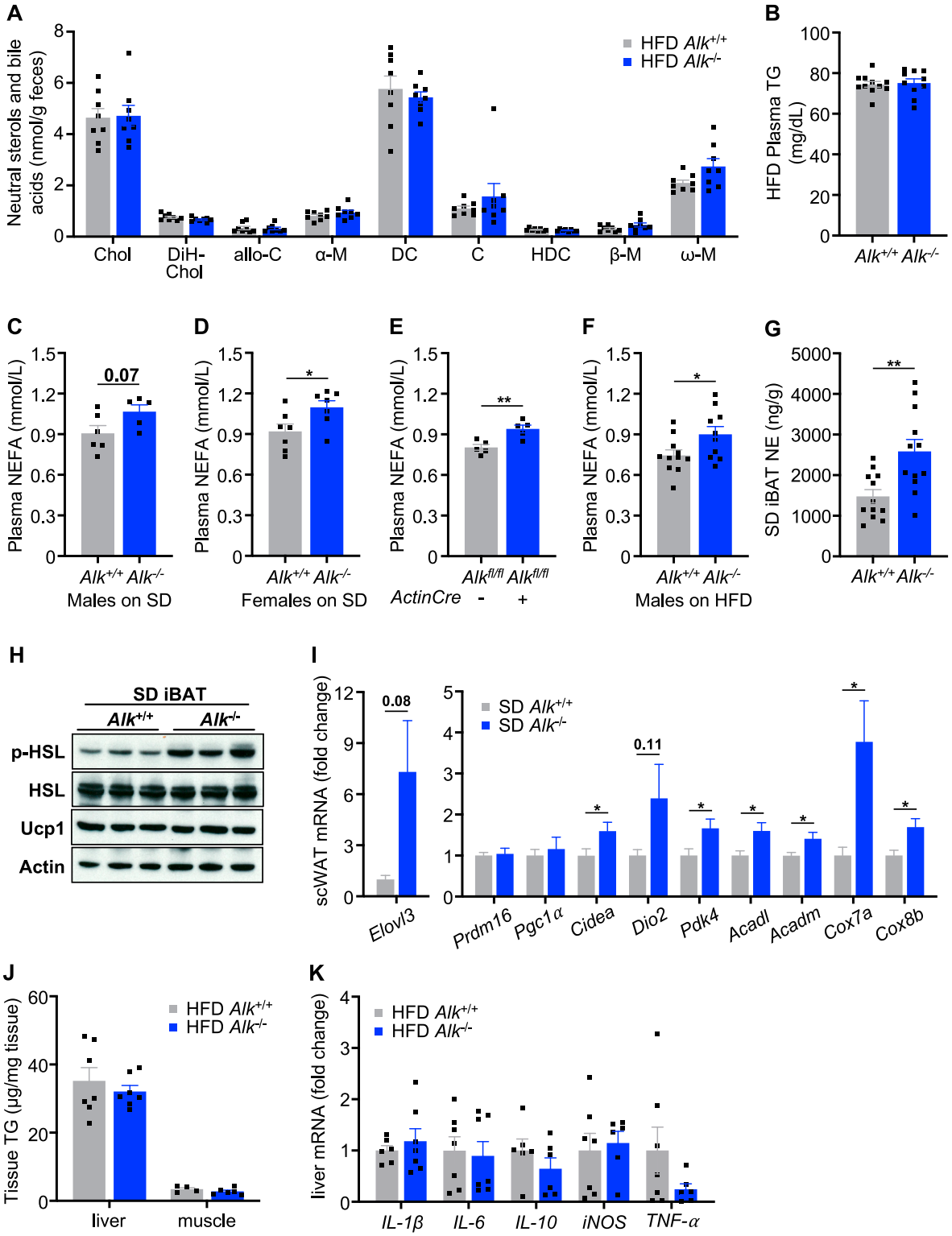

Figure S8. Lipid and Gene Expression Analysis, Related to Figure 6

(A) Quantification of neutral sterols and bile acids contents in the feces of HFD fed mice (n ≥ 8). Chol, cholesterol; DiH-Chol, dihydrocholesterol; allo-C, allocholic acid; α-M, alpha-muricholic acid; DC, deoxycholic acid; C, cholic acid; HDC, hyodeoxycholic acid; β-M, beta-muricholic acid; ω-M, omega-muricholic acid. (B) Quantification of plasma triglycerides (TG) in HFD fed *Alk* knockout and littermate control mice (n ≥ 10). Plasma non-esterified fatty acids (NEFA) levels of male and female SD-fed *Alk* knockout mice (C and D), our second *Alk* knockout mouse line $Alk^{fl/fl}$ $ActinCre^{+}$ (E) and HFD-fed $Alk^{-/-}$ mice (F), compared to littermate

(legend continued on next page)

controls. (G) Quantification of norepinephrine (NE) in brown adipose tissue (iBAT) of SD fed mice (n = 12). (H) Immunoblots for phosphorylated hormone-sensitive lipase (p-HSL), total HSL, Ucp1 and, as loading control, Actin on iBAT of SD fed mice. (I) Quantification of thermogenic and mitochondrial gene expression in the scWAT of SD fed $Alk^{+/+}$ and $Alk^{-/-}$ mice. mRNA levels of target genes were normalized to 36B4 expression and data are presented as fold change to $Alk^{+/+}$ ($n \geq 6$). Abbreviations: *Elovl3, elongation of very long chain fatty acids protein 3; Prdm16, PR domain containing 16; Pgc1α, peroxisome proliferator-activated receptor γ coactivator; Cidea, cell death-inducing DNA fragmentation factor, alpha subunit-like effector A; Dio2, deiondinase, iodothyronine, type II; Pdk4*, *pyruvate dehydrogenase kinase 4*; *Acadl*, *acyl-CoA dehydrogenase long chain*; *Acadm*, *acyl-CoA dehydrogenase medium chain*; *Cox7a, cytochrome c oxidase subunit 7A1* and *Cox8b, cytochrome c oxidase subunit 8B*. (J) Analysis of liver and muscle triglyceride levels of HFD fed animals ($n \geq 4$). (K) Quantification of inflammatory marker gene expression in the liver of HFD fed $Alk^{+/+}$ and $Alk^{-/-}$ mice. mRNA levels of target genes were normalized to *Rpl4*, *Oaz1* and *Rpl13a* expression and data are presented as fold change to $Alk^{+/+}$ ($n \geq 6$). Abbreviations: *IL-1β, interleukin 1 beta; IL-6, interleukin 6; IL-10, interleukin 10; iNOS, nitric oxide synthase; TNF-α, tumor necrosis factor-alpha*. Data are presented as mean ± SEM.; $^{*}p < 0.05$, $^{**}p < 0.01$; Student's two tailed, unpaired t test (B-G and I-K) or 2way ANOVA followed by Bonferroni's multiple comparisons test (A).